

Simulations of Chesapeake Bay estuary: Sensitivity to turbulence mixing parameterizations and comparison with observations

Ming Li, Liejun Zhong, and William C. Boicourt

Horn Point Laboratory, University of Maryland Center for Environmental Science, Cambridge, Maryland, USA

Received 9 July 2004; revised 1 August 2005; accepted 12 September 2005; published 2 December 2005.

[1] Regional Ocean Modeling System (ROMS) is used to develop a new three-dimensional hydrodynamic model for the Chesapeake Bay estuary. Hindcast simulations are conducted for 2 years with markedly different annual river discharges and are compared with time series measurements and high-resolution hydrographic data. The model shows skill in reproducing observed temporal variability in sea level height, salinity, and subtidal current. The agreement with observations is better in the normal runoff year 1997 than in the high runoff year 1996. The model qualitatively reproduces the along-channel and cross-channel salinity distributions during low-to-medium runoff periods. However, during high runoff periods it predicts weaker stratification and a more diffuse halocline than shown by observations. This model/data discrepancy is related to the deficiency of turbulent mixing parameterizations in strong stratification. We have experimented with four turbulence closure schemes (Mellor-Yamada/k-kl, k- ϵ , k- ω , and KPP models) in ROMS but found little difference in the model results. However, vertical stratification shows a strong sensitivity to the background diffusivity. The vertical diffusivity inferred from the model is found to be set by the background diffusivity except in the surface and bottom boundary layers where the turbulence schemes produce similar diffusivity distributions. Among the schemes explored, KPP and k-kl scheme with a background diffusivity of 10^{-5} or 10^{-6} $\text{m}^2 \text{s}^{-1}$ provide the best simulations of the Chesapeake Bay estuary. Both the model sensitivity study and model/data comparison highlight the importance of obtaining a more realistic parameterization for turbulence mixing in a strong pycnocline.

Citation: Li, M., L. Zhong, and W. C. Boicourt (2005), Simulations of Chesapeake Bay estuary: Sensitivity to turbulence mixing parameterizations and comparison with observations, *J. Geophys. Res.*, 110, C12004, doi:10.1029/2004JC002585.

1. Introduction

[2] The Chesapeake Bay estuary is made up of a long main stem interacting with a number of tributaries arrayed along its axis (Figure 1a). The main stem stretches for about 320 km from the mouth of the Susquehanna River at Havre de Grace, Maryland, to the seaward end at Cape Charles and Cape Henry, Virginia. It is shallow, with a mean water depth of 6.5 m. However, a deep paleochannel running in the north-south direction dominates the bathymetry in the middle reaches of the main bay. Eight major tributaries (Susquehanna, Patapsco, Patuxent, Potomac, Rappahannock, York, James and Choptank) contribute to most of the river input. The Susquehanna River in the northern extreme of the bay provides approximately one half of the total freshwater input, while the Potomac River provides about 20% of the total runoff and the James River about 13%.

[3] Chesapeake Bay is a partially mixed estuary, featuring a two-layer circulation with net seaward motion in a surface layer and net landward flow in a bottom layer [e.g.,

Goodrich and Blumberg, 1991]. Typical vertical salinity differences of 2–8 stratify the water column, while salinity differences in the longitudinal direction lie between 20 and 30, depending on the fresh water input from rivers [*Carter and Pritchard*, 1988]. The tidally averaged residual flows are of order of 0.1 m s^{-1} . Moreover, the salinity distribution shows large cross-channel variations, especially in the broader reaches in the south end of the bay [*Boicourt*, 1992]. As fresh water plume moves seaward, tending to the Western Shore, high-salinity ocean water moves landward primarily through deep paleochannels. Both tidal and wind mixing play an important role in determining the salinity distribution and residual circulation [e.g., *Carter and Pritchard*, 1988; *Vieira*, 1986]. Compared with other estuaries, tidal forcing in the bay is relatively modest with tidal range rarely exceeding 1 m [*Browne and Fisher*, 1988]. Winds are episodic with dominant periods of 2–7 days. Northwesterly winds dominate in winter months (November–February) whereas southerly winds of several days each are more frequent in the summer. During the fall transition period, strong wind storms can occasionally destratify the entire water column [*Goodrich et al.*, 1987].

[4] With long and narrow topography, the Chesapeake Bay is a challenging place to develop a predictive model.

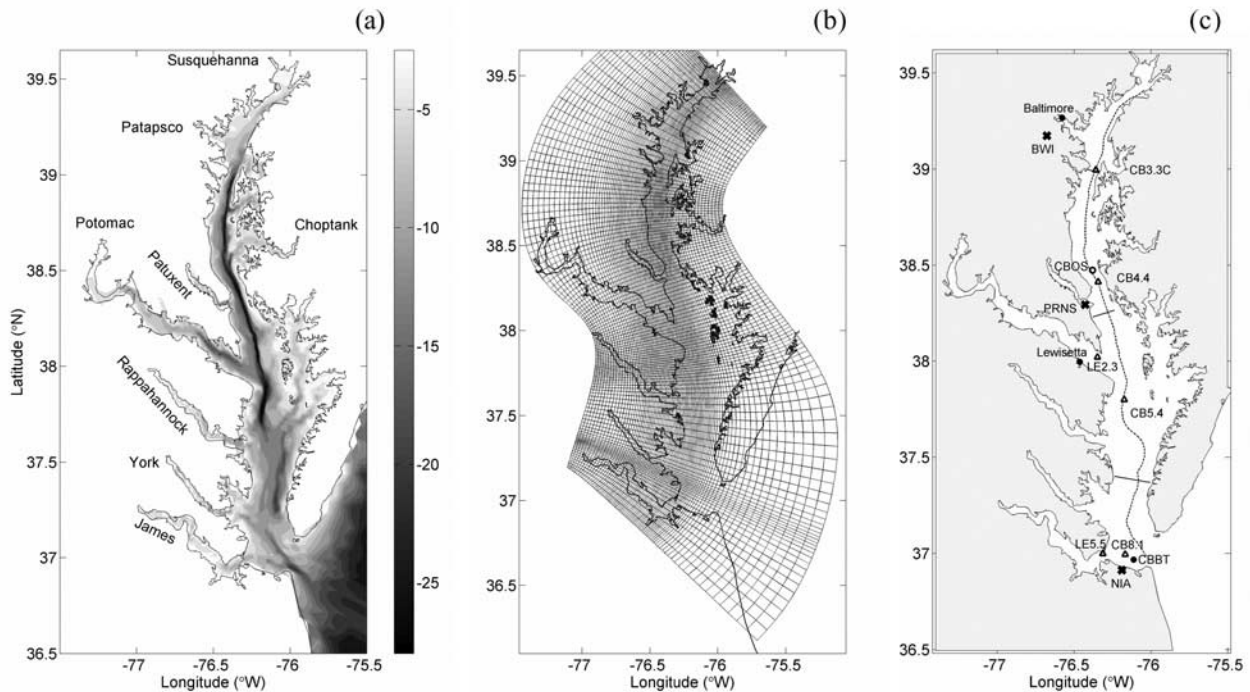


Figure 1. (a) Bathymetry of the Chesapeake Bay and its adjacent coastal area. Major tributaries are marked. Depths are in meters. (b) A horizontal curvilinear coordinate system designed for resolving the complex coastlines and the deep channel in the bay. The model has a horizontal resolution of about 1 km and 20 layers in the vertical direction. (c) Locations for the longitudinal transect and three cross-sectional transects used in the following model analysis. The solid circles are water-level gauge stations and the open circle is the CBOS mid-bay station. The triangle symbols represent CBP monitoring stations CB3.3C, CB4.4, CB5.4, and CB8.1 in the main stem, station LE2.3 in the Potomac River, and station LE5.5 in the James River. The cross symbols represent airport stations where wind measurements were made.

The U.S. Army Corp of Engineers [Johnson *et al.*, 1993; Wang and Johnson, 2000] developed a hydrodynamic model called Curvilinear Hydrodynamics in 3 Dimensions (CH3D). This model incorporates a simple algebraic turbulence closure scheme. Model results have been compared with observations at monitoring stations. Xu *et al.* [2002] found that the model overestimates salinity at depths and the deviation increases toward the lower reaches of the bay. Hence vertical stratification predicted by CH3D is stronger than the observed stratification. Because bottom topography is represented by staircases in the z -coordinate CH3D model, numerical damping generated significant errors, particularly in long estuaries such as the Chesapeake Bay [Xu *et al.*, 2002]. Recently, X. Guo and A. Valle-Levinson (Tidal effects on estuarine circulation in the Chesapeake Bay, submitted to *Journal of Geophysical Research*, 2004) applied the Princeton Ocean Model (POM) to the Chesapeake Bay. They examined the circulation under different combinations of tide, wind and coastal current. Because a constant runoff was imposed in their model, it was difficult to compare their modeled salinity distributions with observations, although the vertical stratification appears to be significantly weaker than observed values. Similar problems with stratification have been reported in numerical simulations of other estuaries.

Several estuarine studies using the Mellor-Yamada closure scheme have noted “runaway” stratification, indicating that turbulence within the stratified interior was underestimated during relatively stable conditions [e.g., Simpson and Sharples, 1991; Monismith *et al.*, 1996]. In order to obtain a realistic prediction for vertical stratification, an accurate turbulence mixing parameterization scheme is essential.

[5] The Regional Ocean Modeling System (ROMS) is a state-of-the-art regional ocean model that has found wide-ranging applications, including basin-scale ocean circulation in the North Atlantic basin [Haidvogel *et al.*, 2000] and shelf circulation in the California Current System [Marchesiello *et al.*, 2003]. On a smaller scale, MacCready and Geyer [2001] and MacCready *et al.* [2002] used ROMS to investigate salt balance in an idealized estuary. We have configured ROMS for the Chesapeake Bay estuary. A number of turbulence parameterization schemes have been incorporated into ROMS [Warner *et al.*, 2005a]. We will experiment with these schemes and examine model’s sensitivity to the turbulence parameterization. Through these sensitivity experiments, we hope to identify key model parameters that control the prediction of vertical stratification and salinity distribution in the Chesapeake Bay. Warner *et al.* [2005b] applied ROMS to the Hudson River estuary

and examined the sensitivity of their model results to turbulence parameterization. They found that the differences between various turbulence closure schemes were much smaller than the differences between any of the simulations and the data. We shall compare our model results with their findings. Although both the Hudson River and Chesapeake Bay are partially mixed estuaries, they are subject to different forcing conditions. Tidal forcing is much stronger in the Hudson River than in the Chesapeake Bay. Wind forcing plays an important role in the Chesapeake Bay but less so in the Hudson River. Thus it is interesting to assess the effectiveness of turbulence schemes in simulating mixing in two different estuaries.

[6] The Chesapeake Bay undergoes large fluctuations in annual river discharge. A major motivation for developing and improving hydrodynamic models is to better understand how interannual variability in river runoffs and nutrient loading affects plankton production and water quality in the Chesapeake Bay [e.g., *Harding et al.*, 2002]. A successful hydrodynamic model should be able to simulate the estuarine circulation under different hydrological forcing conditions. In this paper, we shall carry out hindcast simulations for 2 years: 1996 which has high runoff and 1997 with the annual discharge close to the historical average. Model results will be compared with time series data collected at the monitoring stations and high-resolution salinity distributions obtained during rapid, undulating towed vehicle surveys. Model/data comparison provides a quantitative assessment of the model's predictive skill and may point to aspects of model's parameterizations or forcing data that need refinement. The plan for this paper is as follows. In section 2 we describe the model configuration. Using 1996 as an example, we present model results on the tidally averaged circulation in section 3 and examine the sensitivity to turbulence mixing parameterizations in section 4. Section 5 is devoted to comparisons with spatially resolved salinity distributions obtained during hydrographic surveys, while section 6 will focus on comparisons with time series measurements of sea level, salinity and subtidal current at monitoring stations.

2. Configuration of ROMS for the Chesapeake Bay

[7] We have configured ROMS for the Chesapeake Bay. Bathymetry in the bay is extracted from the high-resolution Coastal Relief Model data archived at NOAA's National Geophysical Data Center. Figures 1a and 1b show the model's bathymetry and grid. The model domain is made much wider than the main stem of the bay in order to include all major tributaries and a part of the coastal ocean to facilitate free exchange across the bay mouth. An orthogonal curvilinear coordinate system is designed to follow the general orientation of the deep channel and the coastlines of the main stem. Coastal boundaries are specified as a finite-discretized grid via land/sea masking. The grid spacing is less than 1 km in the cross-channel (latitudinal) direction and about 2–3 km in the along-channel (longitudinal) direction. The total number of grid points is 120×80 . High resolution is placed in the main stem of the bay to ensure adequate resolution over the deep channel which is the main conduit

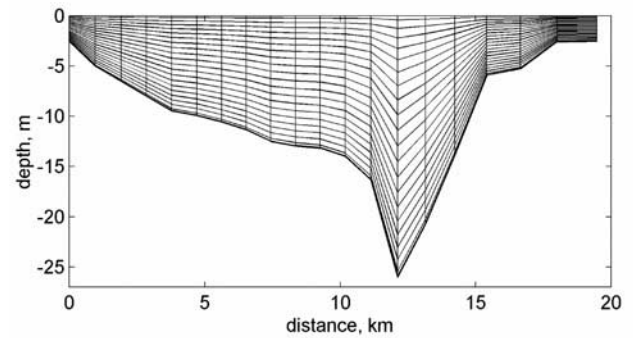


Figure 2. Vertically stretched terrain following coordinates in a midbay cross section.

for landward salt transport. Bottom topographic irregularities with horizontal scales smaller than the grid sizes are truncated by the model. The model has 20 layers in the vertical direction. The stretching parameters for the vertical grid are $\theta_S = 2$ and $\theta_B = 0.8$, as defined in the S-coordinate system [*Song and Haidvogel*, 1994]. Figure 2 shows the vertically-stretched terrain-following coordinates in a mid-bay cross section. A quadratic stress is exerted at the bed, assuming that the bottom boundary layer is logarithmic over a roughness height of 0.5 mm [see *Xu et al.*, 2002]. The vertical eddy viscosity and diffusivity are computed using turbulence mixing schemes incorporated into ROMS. Coefficients of horizontal eddy viscosity and diffusivity are set to $1 \text{ m}^2 \text{ s}^{-1}$.

[8] The model is forced by open ocean tides, freshwater inflows at river heads, wind and heat exchange across the water surface. At the open ocean boundary, sea level was updated using data from stations at Wachapreague, Virginia, and Duck, North Carolina, obtained from NOS (National Ocean Service), NOAA. These coastal sea level data were extrapolated onto the offshore open boundary on the basis of Green's law [*Ippen*, 1966]. The open-ocean boundary condition for the barotropic component consists of a Chapman's condition for surface elevation and a Flather's condition for barotropic velocity. The boundary condition for the baroclinic component includes an Orlandi-type radiation condition for baroclinic velocity and a combination of radiation condition and nudging (with a relaxation timescale of 1 day) for temperature and salinity [*Marchesiello et al.*, 2001]. Salinity and temperature fields on the offshore open boundary were prescribed using monthly Levitus climatology [*Levitus*, 1982] combined with field data at Duck, North Carolina, acquired by the Field Research Facility of the U.S. Army Corps of Engineers. At the upstream boundary in the eight major tributaries, the daily freshwater inflow with zero salinity and time-varying temperature was prescribed. On each inflow cross section, the incoming current is uniform with time-varying speeds regulated by the daily freshwater discharge rate.

[9] The Environmental Protection Agency Chesapeake Bay Program (EPA CBP) serially occupies 88 monitoring stations throughout the bay on at least a monthly schedule. We have constructed a sea surface temperature field using

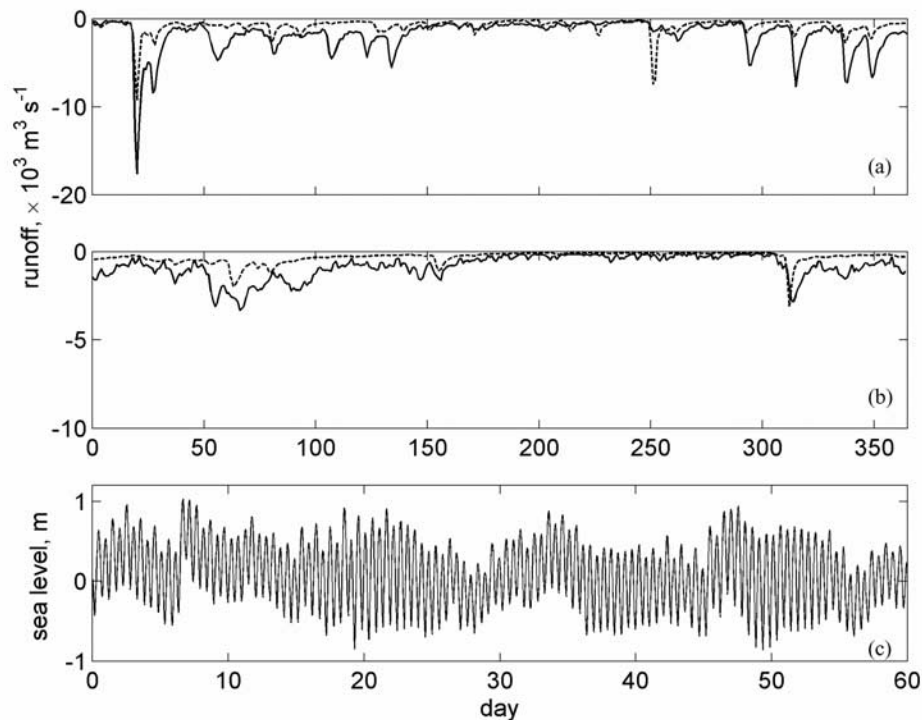


Figure 3. Time series of river discharges during (a) the high runoff year of 1996 and (b) the normal runoff year of 1997 at the Susquehanna River (solid line) and Potomac River (dashed line). (c) Offshore sea level record.

temperature measurements at these monitoring stations. Modeled sea surface temperature is relaxed toward this temperature field with a fast timescale of 6 hours. Hourly wind stress in the lower and middle reaches of the bay was linearly interpolated from data at the Norfolk International Airport (NIA), Patuxent River Naval Station (PRNS) and Baltimore-Washington International Airport (BWI) (see Figure 1c for their locations). North of BWI, the wind stress is assumed to be identical to that at BWI. Wind speeds tend to be stronger over the bay's surface than over land. Empirical amplification factors have been suggested for extrapolating winds over land to winds over water [c.f. Goodrich, 1985; Blumberg and Goodrich, 1990]. Xu *et al.* [2002] and Wang and Johnson [2000] used these empirically adjusted wind data in their simulations of the Chesapeake Bay. We have compared wind measurements obtained at the PRNS airport with those collected at the nearby midbay buoy of the Chesapeake Bay Observing System (CBOS). The empirical amplification factors generated abnormally high wind stress during strong wind events (see section 5 for more discussions). Hence we will conduct two parallel model runs and drive the hydrodynamic model using both the airport winds and the empirically adjusted wind field. Ideally, meteorological stations over the water are desirable, but few buoys were available in 1996 and 1997. Although the CBOS buoys measured wind speeds and directions, they did not cover the whole longitudinal extent of the bay, and contained data gaps, particularly during the winter ice season. Since significant differences in wind speeds are found between the airport

stations surrounding the bay, the hydrodynamic model needs to take the spatial variability of wind field into account. In constructing the wind field for the bay model it should be noted that longitudinal winds are much more effective than lateral winds in driving the circulation along the main stem of the bay [Wang, 1979a, 1979b]. The linear interpolation among the three meteorological stations (NIA, PRNS and BWI) is intended to improve spatial resolution of longitudinal winds along the main axis of the bay.

[10] We have run the model for years 1996 and 1997 using the observed stream flows, tidal forcing and wind field. Figure 3a shows the time series of river discharges at the two largest tributaries, the Susquehanna and Potomac Rivers. There was a series of high runoff events during the spring and fall seasons in 1996. Figure 3b shows the discharges at the two tributaries during 1997. The total discharge from all the tributaries is $4.6 \times 10^{10} \text{ m}^3$ in 1997, which is about one half of the annual river runoff (about $1.0 \times 10^{11} \text{ m}^3$) in 1996. Figure 3c shows the offshore sea level record. It includes all tidal harmonics as well as sea level setup and setdown due to coastal winds. To initialize the model simulation for 1996, we run the model for 1995 using the observed forcing data for that year. Model outputs at the end of 1995 are used to set the initial condition for the salinity and temperature fields. The initial velocity field was taken to be zero, and the water surface was set at the mean sea level. The model has an internal time step of 120 seconds and an external time step of 2 s. Equations are time discretized using a third-order accurate predictor (Leapfrog)

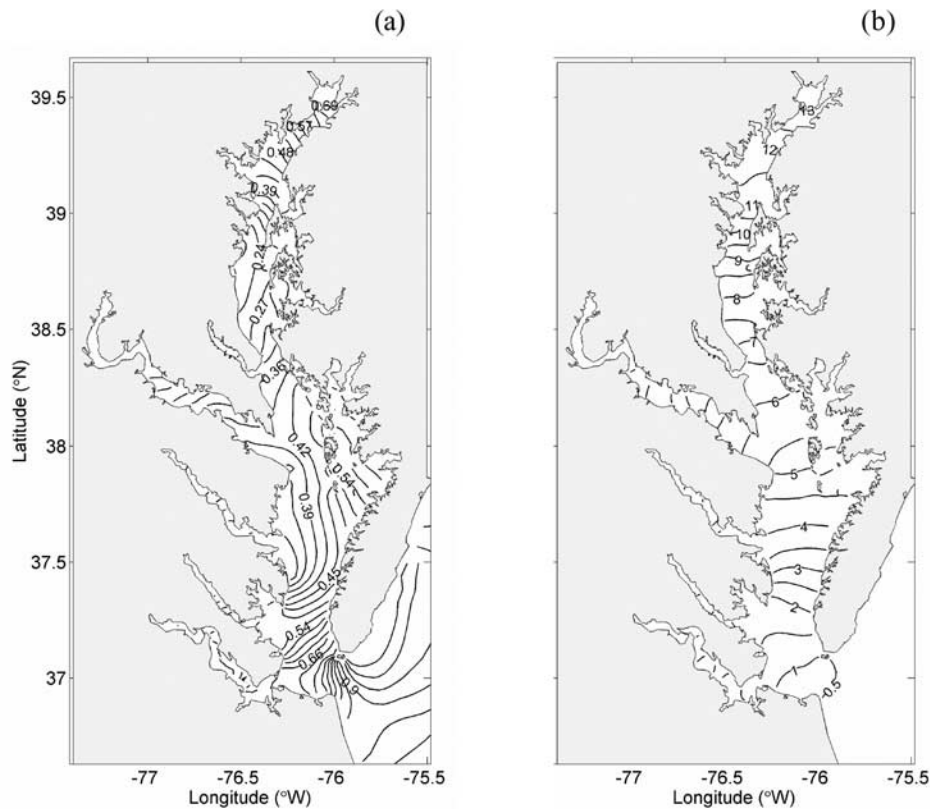


Figure 4. (a) Corange and (b) cophase lines of the semidiurnal M_2 tide predicted from the ROMS model.

and corrector (Adams-Molton) time stepping algorithm which is very robust and stable.

3. Characteristics of Tidally Averaged Residual Circulation

[11] We have conducted model simulations with and without wind forcing. Because episodic wind events complicate the interpretation of estuarine dynamics, we shall examine model results without the wind forcing in sections 3 and 4 and use the results from 1996 as an example. In sections 5 and 6 we will add wind forcing to the model and compare the model results with observational data obtained from both 1996 and 1997. *Warner et al.* [2005a] have incorporated a number of turbulence closure schemes into ROMS. In this section, we shall use the Mellor-Yamada 2.5 scheme with a modified wall function developed by *Burchard et al.* [1998] (this scheme is called k-kl scheme by *Warner et al.* [2005a]) and choose the background diffusivity to be $10^{-5} \text{ m}^2 \text{ s}^{-1}$.

[12] Because tidal currents provide a major source of mechanical energy to the Chesapeake Bay, we first examine model's prediction for tides. The dominant tidal constituent in the Chesapeake is the semidiurnal lunar tide M_2 . Figure 4a shows the corange lines of M_2 tide extracted from the ROMS model. Tidal range is about 1 m at the bay entrance and decreases progressively to about 0.3 m at the upper Bay, near Baltimore [*Browne and Fisher, 1988*]. The tide propagates into the bay as a Kelvin wave, resulting in

larger tidal range on the east side of the bay. Due to bottom friction, tidal amplitude decreases as the tidal wave moves north. In the upper bay north of the Bay Bridge, however, friction and reflection result in wave characteristics which are intermediate between those of a purely progressive tide and those of a standing wave. Tidal amplitude increases toward the head of the estuary, reaching a maximum of about 0.7 m. Figure 4b shows the cophase lines of M_2 tide. It takes about 14 hours for the tidal wave to travel from the mouth to the head. An entire tidal wave can thus be placed inside the bay. The northernmost region of the bay is at the same phase of the tidal cycle as the southernmost region near the mouth. The cotidal and corange lines predicted by the ROMS model are in good agreement with those obtained from water-level gauges and a data-assimilative barotropic model [*Browne and Fisher, 1988; Spitz and Klinck, 1998*].

[13] As a partially mixed estuary, the Chesapeake Bay features a two-layer circulation. The ROMS model reproduces this circulation pattern. Figure 5 shows distributions of salinity and residual velocity along the axis of Chesapeake Bay (see Figure 1c for the geographic location of this longitudinal transect). Both salinity and longitudinal velocity are averaged over the month of April to filter out the tidal effects. Isohalines in the upper reaches of the estuary appear to be vertical, reflecting strong vertical mixing in this shallow region (see Figure 9 in section 4 for model-inferred eddy diffusivity). South of 39.3 latitude, isohalines slope upward toward the sea, as is shown in Figure 5a. Owing to

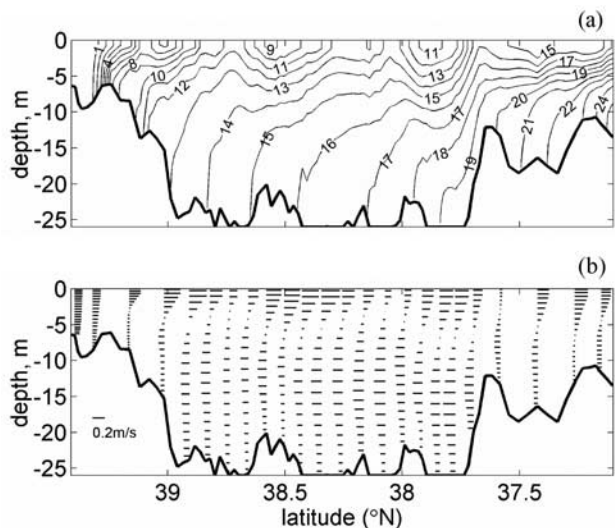


Figure 5. Distributions of monthly averaged (April, 1996) (a) salinity and (b) longitudinal velocity in an along-channel vertical section.

strong tidal mixing in the bottom boundary layer, isohalines are nearly vertical near the bottom. Top-bottom salinity differences in the middle and lower reaches of the bay vary between 5 and 8, while the head-mouth salinity difference lies between 20 and 25. The longitudinal salinity difference in the deep channel (between 37.7 and 39 latitudes) is

around 10. Figure 5b shows the axial component of the residual velocity. Water moves seaward in the surface layers and landward in the bottom layers. Maximum residual velocity is about 0.2 m s^{-1} . The level of no motion separating the two counter-flowing layers lies somewhere between 5 and 8 m. The landward flow in the deep channel reaches the maximum speed at a depth of 15 m, well above the bottom.

[14] Figure 6b shows salinity distribution at the Chesapeake Bay surface, again averaged over the month of April. Fresh water originating from the Susquehanna River moves seaward, tending toward the Western Shore and mixing with the saline oceanic water below. This low-salinity water is joined by the fresh water from the Potomac River as it continues its way seaward. This plume expands laterally in the lower bay before exiting as a buoyancy-driven current along the coast [Chao and Boicourt, 1986]. The high runoff of 1996 decreases surface salinities at the mouth of the bay to values near 20. Salinity outside the bay plume is higher so that there is a strong lateral salinity gradient near the bay mouth. Similar lateral gradients have been reported from observations [e.g., Carter and Pritchard, 1988].

[15] Two hypotheses have been proposed to explain this east-west asymmetry in the surface salinity distribution: (1) the Coriolis force holds the fresh water plume against the Western Shore as it moves seaward; (2) most river tributaries are located on western side of the Chesapeake Bay and discharge fresh water onto the Western Shore [c.f. Carter and Pritchard, 1988]. We have tested these hypotheses by carrying out a model run in which the Coriolis

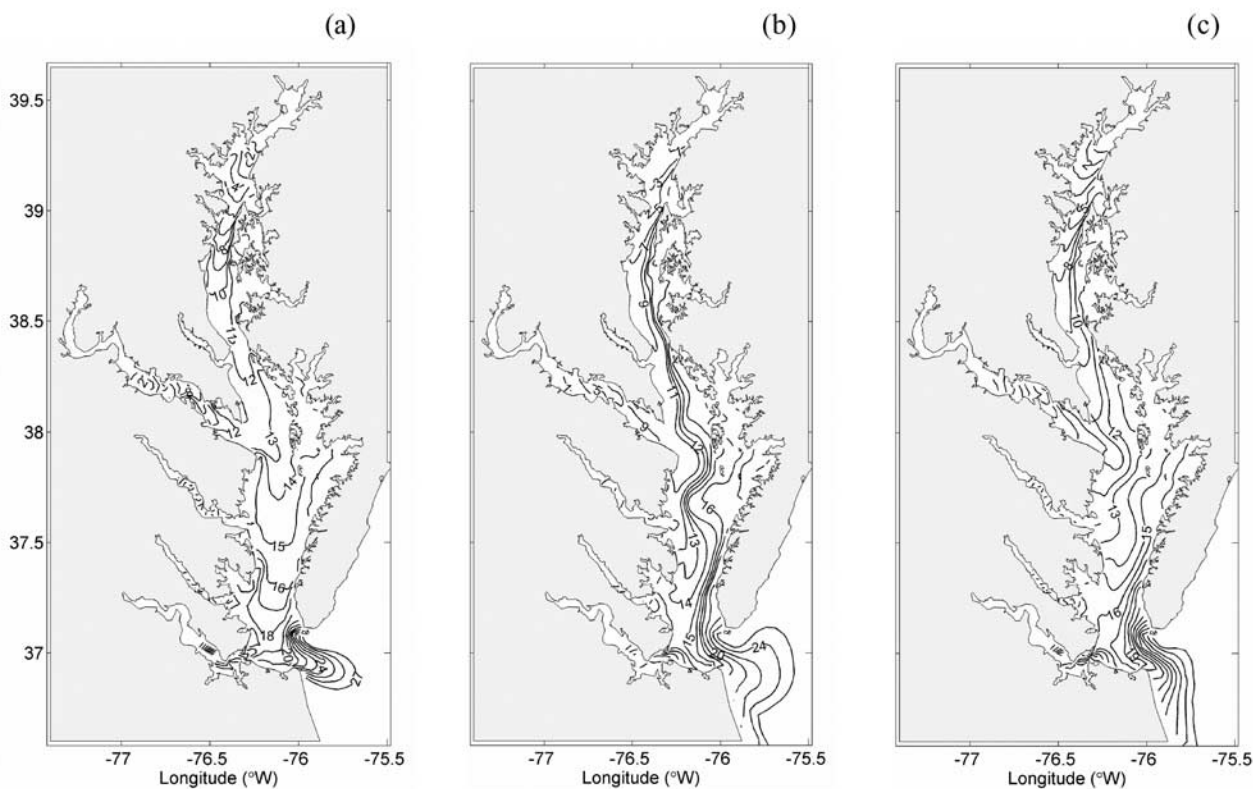


Figure 6. Sea-surface salinity in April 1996 for three runs: (a) without the Coriolis force and wind; (b) with the Coriolis force but without wind; and (c) with both the Coriolis force and wind.

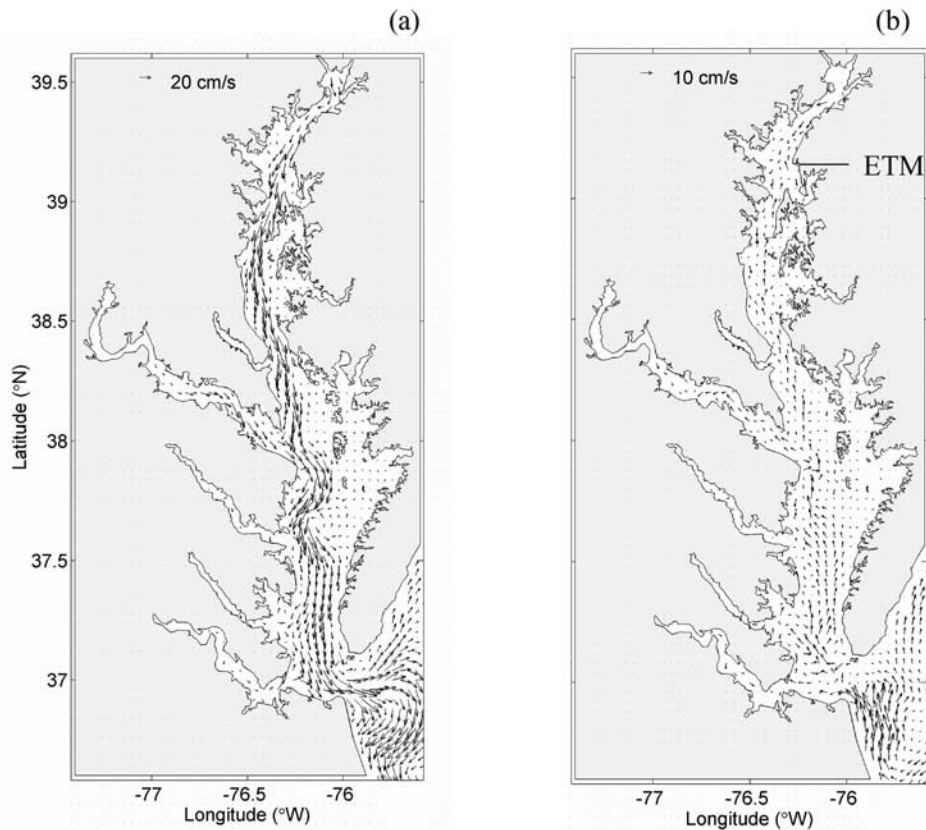


Figure 7. Tidally averaged (over the month of April 1996) residual flow (a) at the sea surface and (b) at 2 m above the bottom.

force is switched off. As shown in Figure 6a, the fresh water plume originated from the Susquehanna River now moves faster in middle of the bay surface. More tellingly, the plume originated from the Potomac River moves across the

bay surface to join the Susquehanna plume there. The combined plume continues to move seaward along the center axis of the bay. Because frictional resistance is higher in shallow shoal regions, buoyant water moves faster in

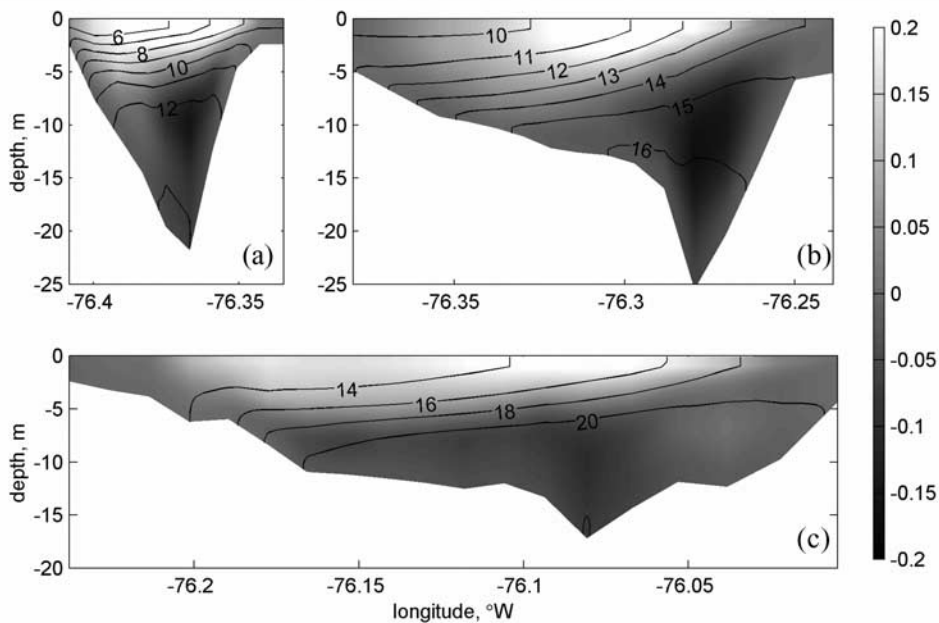


Figure 8. Monthly averaged (April 1996) salinity distribution (contours) and residual velocity (shading) at three cross sections: (a) upper bay, (b) middle bay, and (c) lower bay.

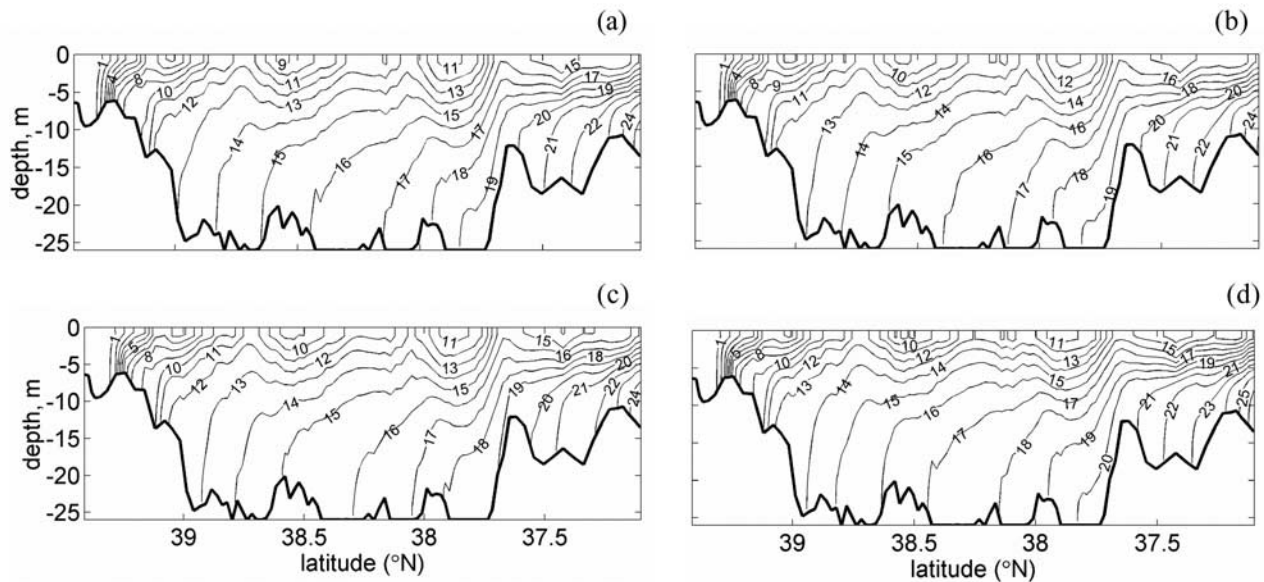


Figure 9. Sensitivity of April's along-channel salinity and residual velocity distributions to turbulence mixing schemes. (a) Mellor-Yamada ($k-k_1$) scheme, (b) $k-\omega$ scheme, (c) $k-\epsilon$ scheme, and (d) KPP model.

deep water so that the plume appears to be advancing along the center axis of the bay. Without the constraint of the Coriolis force, the low-salinity plume spreads in the offshore direction after exiting the bay mouth. The comparison between Figures 6a and 6b have clearly demonstrated that the Coriolis force causes the east-west asymmetry of salinity distribution at the bay surface. Lateral tilts in isohalines are larger in the model than in observations, particularly in the upper bay. In Figure 6c we show the surface salinity distribution from a model run that includes both the Coriolis force and wind forcing. Isohalines in the upper bay show less tilt. Moreover, the lateral front separating the fresh water plume from the ambient water is diffused. Thus it appears that wind-induced mixing and stirring smooth out lateral salinity gradients and affect the spreading of the seaward flowing fresh water in the Chesapeake Bay.

[16] We have discussed the two-layer residual circulation in a vertical section aligned with the center axis of bay. Now we examine the horizontal patterns of residual currents at the sea surface and at 2 m above the bottom (Figure 7). Consistent with the two-layer circulation, the surface current is directed seaward whereas the bottom current is directed landward. However, currents show considerable spatial variability. The surface current is visibly stronger in the seaward flowing low salinity water (see Figure 7a). This jet-like current generally follows the coastline of the Western Shore but spreads over the full channel width in the lower bay (south of 37.5 degrees) before it exits the bay mouth as a plume and buoyancy-driven coastal current in the far field. The bottom current is generally directed landward but is highly variable due to interactions with topography, as shown in Figure 7b. High-salinity water enters the bay mouth in the east-west direction and appears to speed up within the south and north channels located near the bay mouth [c.f. *Valle-Levinson and Lwiza, 1995*]. North of 37.3 latitude, the bottom current shifts to the south-north direction as the coastline changes its orientation. The

current moves northward and is slightly stronger in a channel located close to the Eastern Shore (between 37.3 and 37.7 latitudes). In the middle reach of bay, the bottom current follows the deep center channel and transports salt upstream. At a location close to 39.3 latitude, northward and southward flows converge along the bottom. This flow convergence corresponds to the front of the salt wedge or the zone of estuarine turbidity maximum.

[17] In Figure 8 we look at distributions of salinity and tidally-averaged residual velocity at three cross sections, representative of upper, middle and lower bay (see Figure 1c for locations of these cross-channel sections). Section 1 is a narrow section with a triangular shape typical of upper bay. Section 2 is a typical middle bay section with a deep channel in the center. Section 3 is a wide and shallow section typical of lower bay. Owing to the effects of Coriolis force, the isohalines in all vertical cross sections are tilted down toward the Western Shore. Hence there are large cross-channel salinity gradients, as reported in observations [*Boicourt, 1992*]. The tidally averaged residual currents show a seaward flow in the surface layer and a landward flow in the bottom layer. The level of no motion separating the two flow layers is tilted in a way similar to isohalines. While the seaward flow reaches its maximum speed at the sea surface, the landward flow is fastest at a midpoint in the bottom layer. Diagnostics presented in this section have shown that the ROMS model can qualitatively capture key characteristics of tidally averaged salinity distribution and estuarine circulation as revealed in previous observations of the Chesapeake Bay. A quantitative assessment of the model results will be conducted in sections 5 and 6.

4. Sensitivity to Turbulence Mixing Parameterization

[18] Because turbulent mixing plays a critical role in determining the stratification and residual circulation in

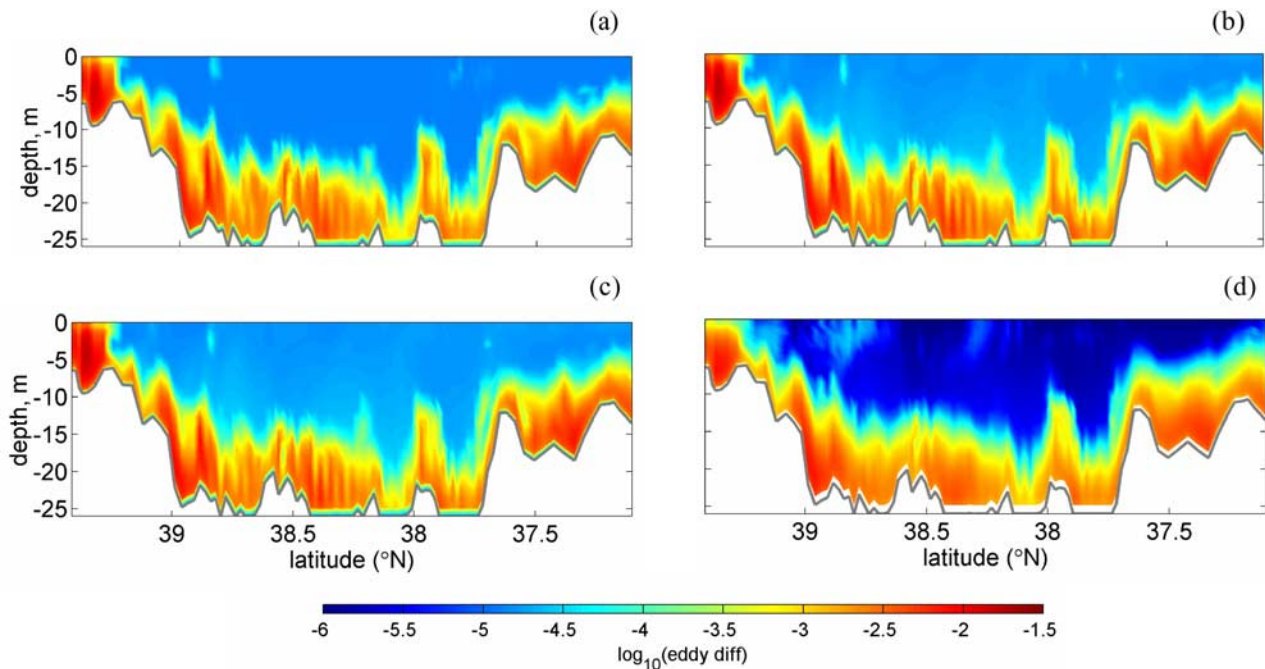


Figure 10. Eddy diffusivity in an along-channel section for four turbulence mixing schemes. (a) Mellor-Yamada (k-kl) scheme, (b) k- ω scheme, (c) k- ϵ scheme, and (d) KPP model.

estuaries, we shall examine the sensitivity of the model results to turbulence mixing parameterization. Model sensitivity to turbulence parameterization has been examined in idealized oceanic flows. In one-dimensional models, *Umlauf and Burchard* [2003] found that Mellor-Yamada, k- ϵ , k- ω models produce identical predictions for the classic mixed-layer entrainment experiment of *Kato and Phillips* [1969], but only k- ω model computes correct decay rates for turbulence quantities under breaking waves. In three-dimensional models for a steady barotropic flow and an oscillatory stratified pressure-gradient driven flow (estuarine circulation) in a rectangular channel, *Warner et al.* [2005a] tested k- ϵ model, k- ω model, and Mellor-Yamada (k-kl) model with different wall-proximity functions. They found that k- ϵ , k- ω and k-kl model produce similar results on key flow quantities.

[19] Effects of turbulence parameterizations have also been studied in numerical models of the coastal ocean. Using a two-dimensional model, *Wijesekera et al.* [2003] examined the sensitivity of model-produced wind-driven circulation on the continental shelf to turbulence closure schemes. They found that Mellor-Yamada, k- ϵ and KPP schemes predict similar features in the mesoscale circulation field. The schemes produce qualitatively similar eddy diffusivities and eddy viscosities in both upwelling and downwelling simulations, but turbulence structures and mixing intensities can differ quantitatively. *Durski et al.* [2004] found significant differences between the Mellor-Yamada and KPP schemes in some of their numerical experiments. In the one-dimensional mixed layer entrainment experiments, they found that Mellor-Yamada mixes deeper and entrains more than KPP when the pycnocline beneath the mixed layer is highly stratified but mixes less when it is weak. In two-dimensional

numerical experiments of coastal upwelling circulation, they found minor difference under strong stratification conditions but major differences under weak stratification conditions. They suggested that the differences in the model results are related to how each scheme parameterizes the dependence of vertical mixing on the gradient Richardson number.

[20] These sensitivity studies indicated that turbulence parameterization schemes may perform differently in different flows. It is thus important for us to find out how they perform in a realistic model of the Chesapeake Bay estuary. More importantly, most of the previous investigations appear to have ignored the background diffusivity, which we find is the most important parameter controlling the mixing and stratification in the interior of an estuary.

[21] *Warner et al.* [2005a] incorporated the generic length-scale turbulence closure scheme of *Umlauf and Burchard* [2003] into ROMS. This scheme includes one equation for turbulent kinetic energy and a second equation for a generic turbulence length-scale quantity. It includes three popular schemes: Mellor-Yamada, k- ϵ and k- ω schemes. In such a two-equation model, turbulent momentum and scalar fluxes are proportional to the local gradients of mean flow and mean scalar concentration. Eddy viscosity K_M and eddy diffusivity K_H are parameterized as

$$K_M = S_M k^{1/2} l + K_{MB} \quad (1)$$

$$K_H = S_H k^{1/2} l + K_{HB}. \quad (2)$$

in which k is the turbulence kinetic energy, l is the turbulence length scale, S_M and S_H are stability functions, K_{MB} and K_{HB} are background viscosity and diffusivity.

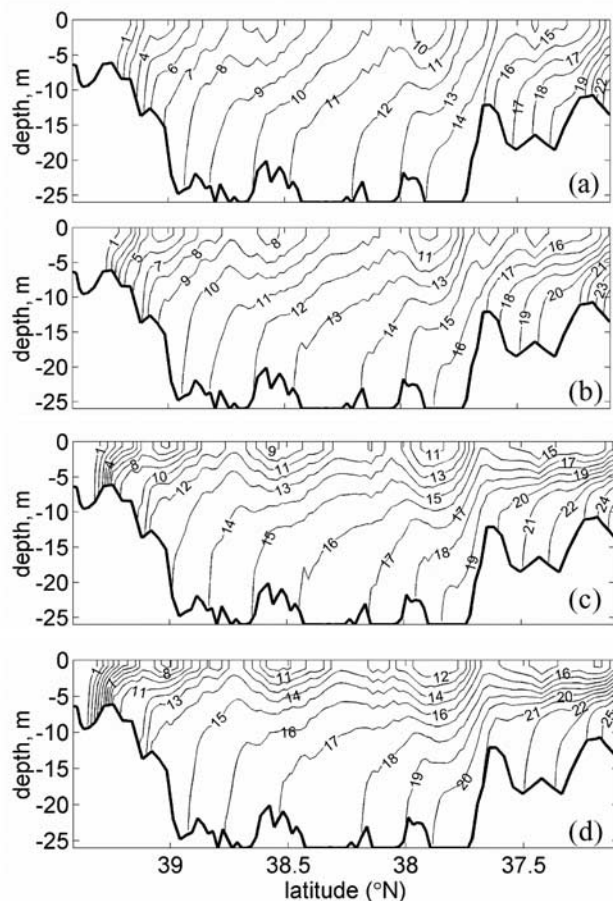


Figure 11. Along-channel salinity distribution at different background vertical mixing coefficient K_{HB} equal to (a) 10^{-4} , (b) 5×10^{-5} , (c) 10^{-5} , and (d) $10^{-6} \text{ m}^2 \text{ s}^{-1}$.

Although there is a consensus on the equation for the turbulence kinetic energy, there is considerable debate on the choice and nature of second equation for determining the turbulence length scale. In the Mellor-Yamada model, the second equation was developed for kl [Mellor and Yamada, 1982]. In the $k-\epsilon$ scheme, an equation for turbulence energy dissipation was constructed [Rodi, 1987]. In the $k-\omega$ scheme, an equation was developed for turbulence frequency [Wilcox, 1988] and was extended to include buoyancy terms for geophysical applications by Umlauf *et al.* [2002]. The Mellor-Yamada scheme requires a wall proximity function to ensure a positive value for the diffusion coefficient. Warner *et al.* [2005a] evaluated four wall proximity functions in an estuary simulation and found that the parabolic shape suggested by Mellor and Yamada [1982] produced different results from the other three functions which produced indistinguishable results. We chose the symmetric linear shape function proposed by Burchard *et al.* [1998]. In order to be consistent with other two-equation models, Warner *et al.* [2005a] designated the Mellor-Yamada Level 2.5 scheme as $k-kl$ scheme.

[22] ROMS also incorporates the K-profile parameterization (KPP) model introduced by Large *et al.* [1994] in which profiles of eddy viscosity and diffusivity are constructed from the Monin-Obukhov similarity theory. ROMS implements the KPP scheme for both surface and bottom

oceanic boundary layers. In the KPP model, turbulence flux consists of a downgradient part and a nonlocal part

$$\overline{-w\bar{x}} = K_x(\partial_z X - \gamma_x), \quad (3)$$

$$K_x(\sigma) = hw_x(\sigma)G(\sigma). \quad (4)$$

in which the nonlocal scalar flux γ_x is based on a formula suggested by Deardorff [1972] and the downgradient eddy diffusivity K_x is parameterized in terms of the boundary depth, a depth-dependent turbulent velocity scale and an empirical nondimensional vertical shape function. Away from the surface and bottom boundary layers, the KPP model is extended to include turbulent mixing due to shear instability associated with the mean flow, internal wave breaking, and double diffusion (which was switched off in the current application).

[23] We now experiment with KPP, $k-kl$, $k-\epsilon$ and $k-\omega$ schemes in the model for the Chesapeake Bay estuary. In the two-equation models ($k-kl$, $k-\epsilon$ and $k-\omega$ schemes), we use the equilibrium stability function of Kantha and Clayson [1994], since Warner *et al.* [2005a] found that this stability function works well in their model simulations of an idealized estuarine circulation in a rectangular channel. The background diffusivity (and background viscosity) is set to be a constant of $10^{-5} \text{ m}^2 \text{ s}^{-1}$, which is a rudimentary way to parameterize mixing due to breaking internal waves. In the KPP model, the parameterization for interior mixing is more sophisticated and includes Richardson-number dependent formula for shear-induced

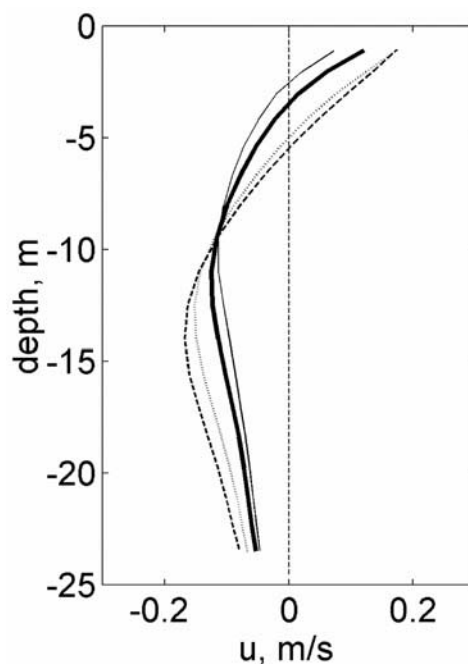


Figure 12. Vertical profiles of tidally averaged along-channel velocity at a midbay station corresponding to background vertical mixing coefficient K_{HB} equal to 10^{-6} (thin solid line), 10^{-5} (thick solid line), 5×10^{-5} (dotted line), $10^{-4} \text{ m}^2 \text{ s}^{-1}$ (dashed line).

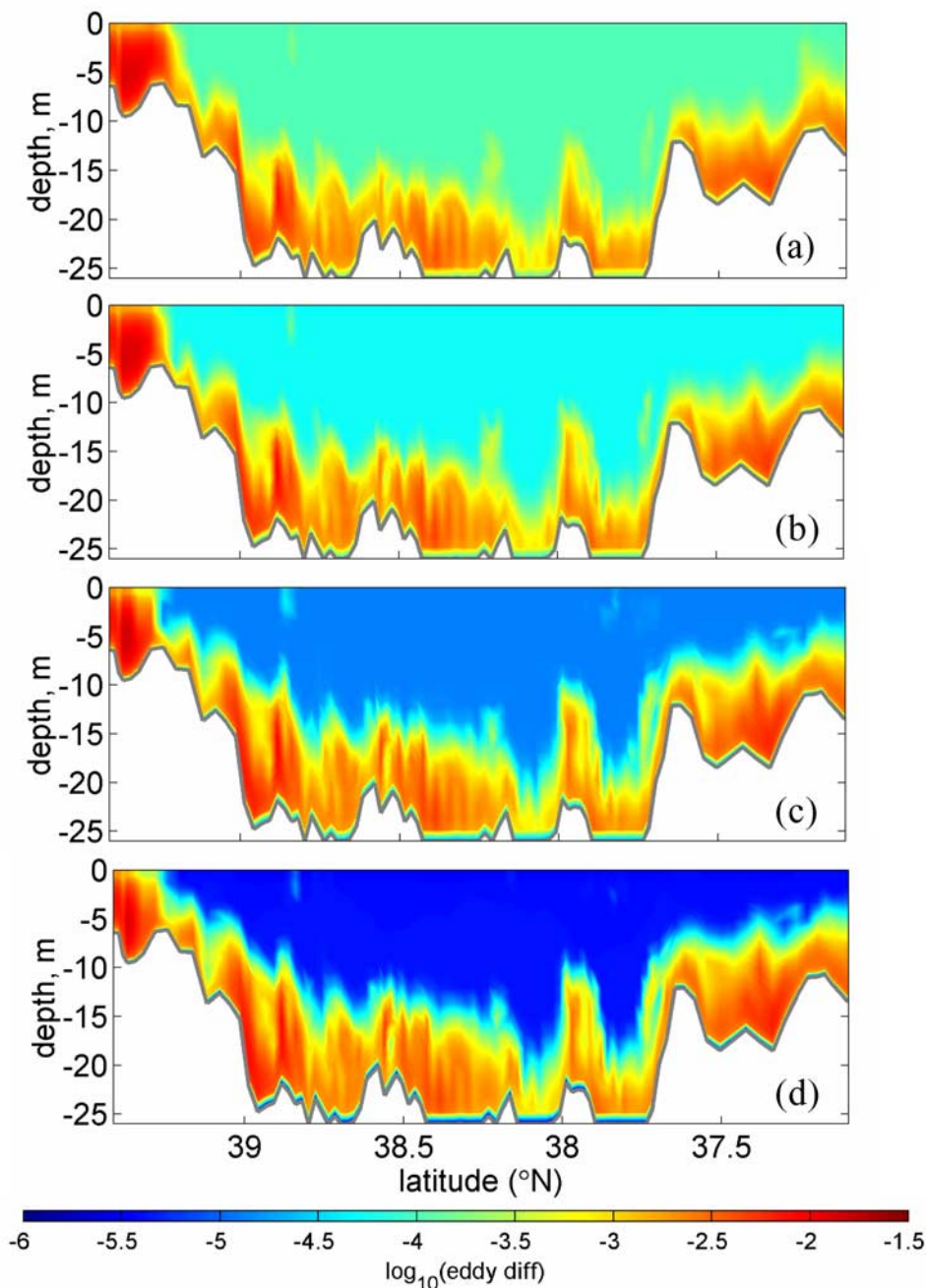


Figure 13. Along-channel distribution of eddy diffusivity at K_{HB} equal to (a) 10^{-4} , (b) 5×10^{-5} , (c) 10^{-5} , and (d) $10^{-6} \text{ m}^2 \text{ s}^{-1}$.

mixing and a stratification-dependent formula for internal wave breaking [Garrett and Holloway, 1984].

[24] Figures 9 and 10 show a comparison of along-channel salinity and diffusivity distributions between the four turbulence schemes. As shown in Figure 9, there are virtually no differences between $k\text{-}kl$, $k\text{-}\epsilon$ and $k\text{-}\omega$ schemes. The KPP model produces slightly different results: low-salinity surface water spreading further downstream, deep saline water intruding farther upstream, and vertical stratification being slightly stronger. This comparison suggests that the four turbulence parameterization schemes perform almost equally well. The reason becomes clear when we

examine the model-inferred eddy diffusivity in the same along-channel section (see Figure 10). All four schemes predict much larger eddy diffusivity in the bottom boundary layer because tidal currents generate strong turbulent mixing there. The maximum diffusivity in the tidal boundary layer reaches between 0.01 to $0.1 \text{ m}^2 \text{ s}^{-1}$. Above the bottom boundary layer, diffusivity is much smaller and indistinguishable from the background value of $10^{-5} \text{ m}^2 \text{ s}^{-1}$ in the two-equation closure models, although it is weaker and close to $10^{-6} \text{ m}^2 \text{ s}^{-1}$ in the KPP model.

[25] On the basis of these comparative model simulations, we can conclude that all four schemes perform equally well

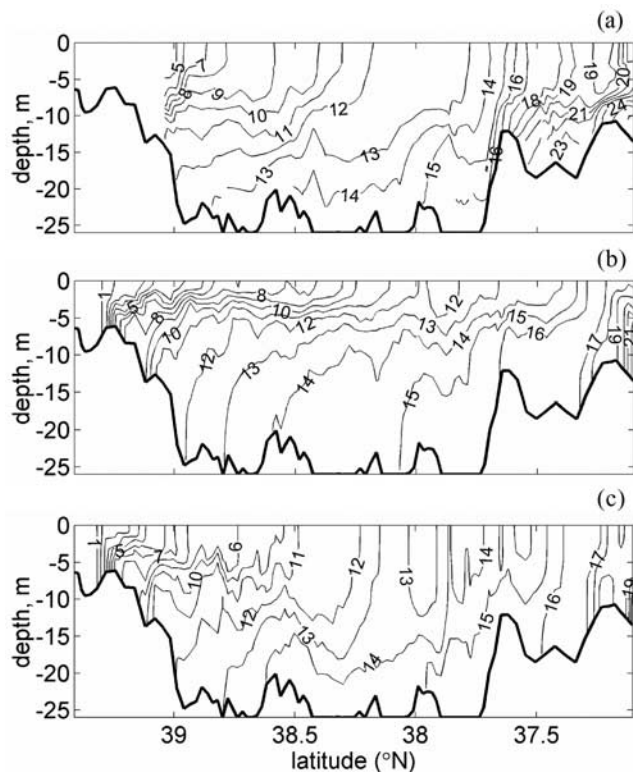


Figure 14. Comparison of along-channel salinity distribution on 1 November 1996 between (a) high-resolution Scanfish measurements, (b) ROMS model with KPP scheme using wind speeds measured at airports, and (c) empirically adjusted wind speeds.

in predicting turbulence in the bottom boundary layer. Consequently, the salinity distributions and residual circulation fields in the estuary are also about the same. Figures 9 and 10 suggest that the model results are not sensitive to different turbulence mixing parameterization schemes. Although we presented the model comparison for the high runoff period, we found the same results at other times when the river runoff is lower. Our results are in agreement with those of *Wijesekera et al.* [2003] for the wind-driven coastal circulations and those of *Warner et al.* [2005b] for the estuarine circulation in the Hudson River. They also found minor differences between different turbulence closure schemes. Although the results of the hydrodynamic model are relatively insensitive to different turbulence parameterization schemes, future research is needed to investigate the sensitivity of sediment transport and biophysical models to turbulence mixing parameterizations.

[26] Next we turn our attention to model's sensitivity to the background diffusivity. It is supposed to parameterize turbulent mixing due to breaking internal waves. To investigate this issue, we use k-kl scheme as an example and run the model with $K_{HB} = 10^{-5}$, 5×10^{-5} and $10^{-4} \text{ m}^2 \text{ s}^{-1}$. The background eddy viscosity K_{MB} is always set to be equal to K_{HB} . Microstructure measurements and tracer release experiments in the open ocean suggest a value of order of $10^{-5} \text{ m}^2 \text{ s}^{-1}$ [Gregg, 1987; Ledwell et al., 1993], while *Munk* [1966] inferred a value of $10^{-4} \text{ m}^2 \text{ s}^{-1}$ from a simple advective-diffusive balance for the main thermo-

cline. For comparison, we have also run a case of super-low mixing coefficient with $K_{HB} = 10^{-6} \text{ m}^2 \text{ s}^{-1}$. Figure 11 shows a comparison of along-channel salinity distribution between the four model runs. The vertical stratification reduces as K_{HB} increases: the top-bottom salinity difference in the midbay decreases from 6 to 2 as K_{HB} increases from 10^{-5} to $10^{-4} \text{ m}^2 \text{ s}^{-1}$. The longitudinal salinity gradient also changes. The slopes of isohalines become steeper as K_{HB} increases, suggesting a transition from a partially mixed estuary to a vertically homogeneous one. However, the comparison between Figures 11c and 11d shows a much smaller change in the vertical stratification as K_{HB} is reduced from 10^{-5} to $10^{-6} \text{ m}^2 \text{ s}^{-1}$. This suggests that the model prediction for vertical stratification becomes relatively insensitive to changes in the background diffusivity when K_{HB} is reduced below $10^{-5} \text{ m}^2 \text{ s}^{-1}$.

[27] The background diffusivity also affects the prediction of the gravitational circulation in the Chesapeake Bay. Figure 12 shows how the vertical profile of the residual velocity changes with K_{HB} at a midbay station. To understand this strong sensitivity to the background diffusivity, we examine the distribution of model-inferred eddy diffusivity in the along-channel section, as shown in Figure 13. Away from the bottom boundary layer, the eddy diffusivity is determined by the prescribed background diffusivity. Therefore it comes as no surprise that the stratification in the interior of the estuary is sensitive to the background diffusivity as K_{HB} effectively controls vertical mixing there. It is interesting to note that the salinity distribution in Figure 11d (k-kl scheme with $K_{HB} = 10^{-6} \text{ m}^2 \text{ s}^{-1}$) is fairly close to that shown in Figure 9d (KPP scheme). The 15 isohaline intersects the bed and sea surface at about the same locations. The deep-water salinity at the estuary mouth is 26 and length of salt intrusion is nearly identical between the two schemes. As shown in Figure 10d, KPP predicts a diffusivity of about $10^{-6} \text{ m}^2 \text{ s}^{-1}$ above the bottom boundary layer. Hence KPP compares best to k-kl with $K_{HB} = 10^{-6} \text{ m}^2 \text{ s}^{-1}$.

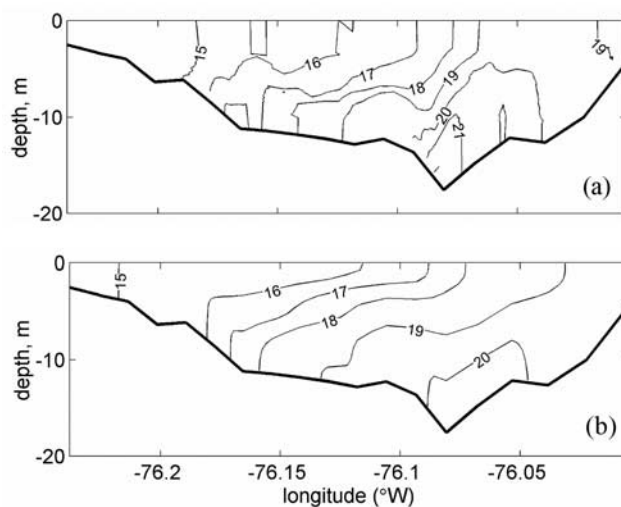


Figure 15. Comparison of the salinity distribution in a lower-bay cross-channel section on 13 November 1996. (a) Observed salinity. (b) ROMS model with k-kl scheme and $K_{HB} = 10^{-5} \text{ m}^2 \text{ s}^{-1}$.

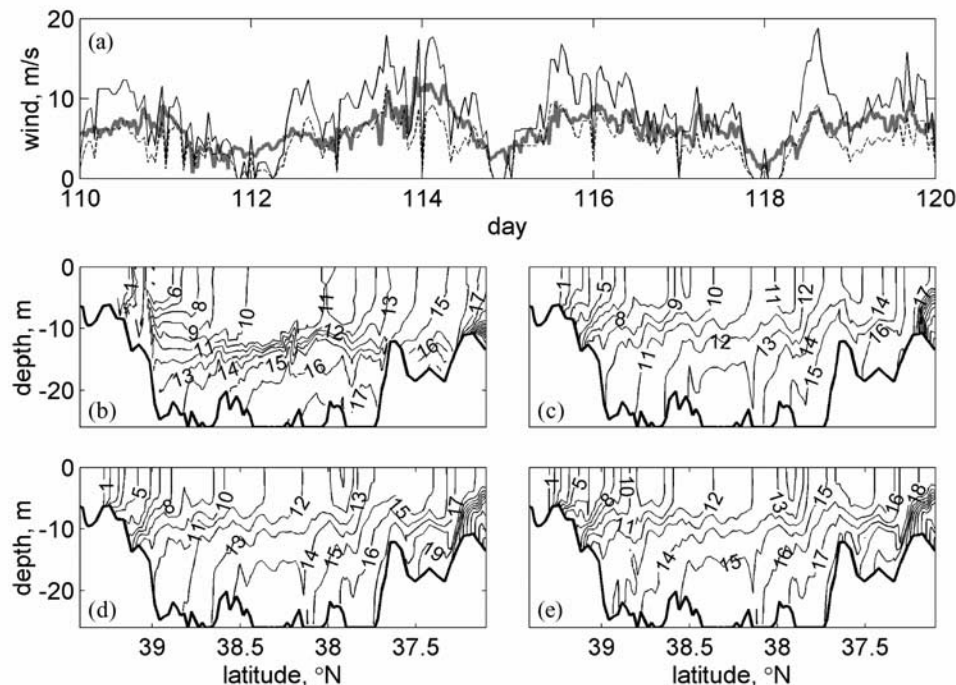


Figure 16. (a) Time series of the wind speed magnitude observed at PRNS airport-recorded (dashed line) and CBOS midbay buoy (thick shaded line) and their comparison with the empirically amplified wind speed (solid line). Comparison of the along-channel salinity distribution on 23 April 1996 (day 114) between (b) high-resolution scanfish measurements, (c) ROMS model with KPP scheme, (d) ROMS model with $K_{HB} = 10^{-5} \text{ m}^2 \text{ s}^{-1}$, and (e) $K_{HB} = 10^{-6} \text{ m}^2 \text{ s}^{-1}$.

[28] We have shown that all of the four turbulence closure schemes are doing a reasonably good job of predicting turbulence mixing in the bottom boundary layer but all fail to produce a mixing coefficient above the prescribed background value in the stratified pycnocline region. We have also shown that the stratification and residual circulation are sensitive to changes in the background diffusivity when it is above $10^{-5} \text{ m}^2 \text{ s}^{-1}$. These model sensitivity experiments point to the importance of understanding and parameterizing turbulence mixing in the stratified pycnocline. When studying vertical exchange within the pycnocline of a salt wedge estuary, *Geyer and Smith* [1987] found that internal waves make an important contribution to the shear instability. Turbulent mixing in stratified flows, such as that caused by breaking internal waves, is intermittent. A physics-based parameterization of this mixing process is required in order to obtain more robust predictions for salinity distributions and residual circulation in estuaries.

5. Structure Comparison

[29] To assess the model's capability in hindcasting circulation in the Chesapeake Bay estuary, we compare model results with observations. In this section we look at snapshots of salinity distributions in along-channel and cross-channel sections. In the next section we shall compare model results with time series measurements at monitoring stations. We focus on the year of 1996 with high runoff, but will also include data from the more typical runoff year of 1997 so that we can evaluate model's performance under varying hydrological forcing conditions. Because winds can

drive significant subtidal currents in the bay and cause turbulent mixing in the surface layer [*Wang*, 1979a, 1979b; *Goodrich et al.*, 1987; *Goodrich*, 1988], we include wind forcing in the model simulations.

[30] The very nature of an estuary, with its semienclosed geometry and freshwater runoff from land drainage sets up strong spatial gradients in water properties and flow fields. In the Chesapeake Bay, the dendritic geometry which was created from river valleys by sea level rise adds to this complexity. We will compare model results with observations, but recognize that the model grid cannot resolve small-scale flow features associated with the complex bathymetry in the bay. In this section we examine salinity distributions across the whole estuary. Large-scale density structures emerging from these spatial maps provide important information on the estuarine dynamics, although strong wind events may alter them on short timescales. In a project supported by the National Science Foundation, the TIES (Trophic Interactions in Estuarine Systems) field program produced detailed three-dimensional views of temperature, salinity, chlorophyll, dissolved oxygen and zooplankton abundance in the bay. Field surveys were conducted each year in three seasons (April, July, October), employing a Scanfish towed undulating vehicle equipped with multiple sensors. While the Scanfish was towed at approximately 7 knots, it undulated with a typical wavelength of 300 m and transited the 300-km length of the estuary in less than 30 hours. A series of lateral transects complemented this axial view. This towed vehicle technique provided a nearly-synoptic, three-dimensional view of the density structure of the bay that had never been achieved before.

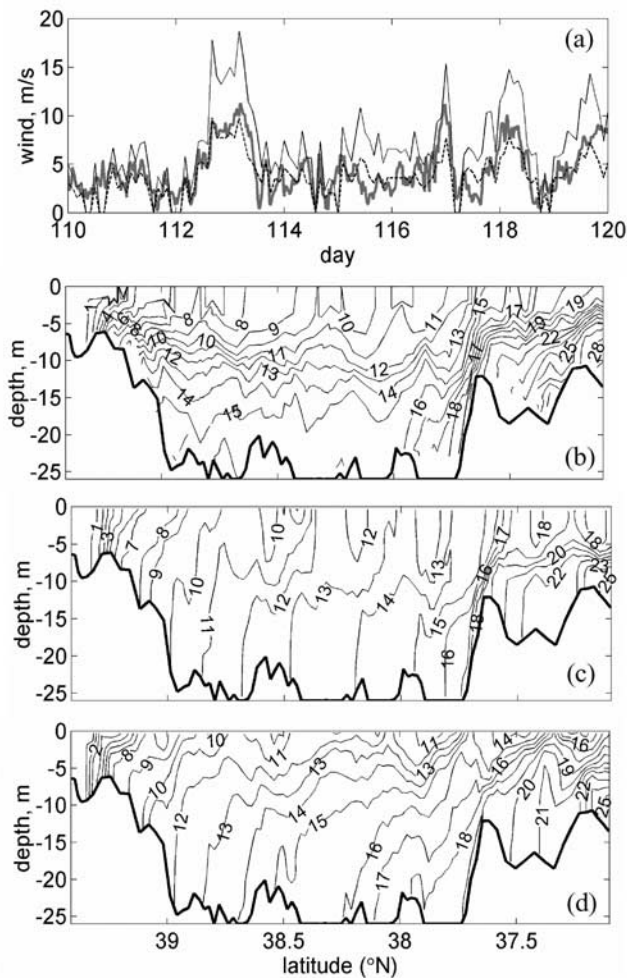


Figure 17. (a) Time series of the wind speed magnitude observed at PRNS airport (dashed line) and CBOS midbay buoy (thick shaded line) and their comparison with the empirically amplified wind speed (solid line). Comparison of the along-channel salinity distribution on 25 April 1997 (day 115) between (b) high-resolution Scansfish measurements, (c) ROMS model with k-kl scheme using amplified winds, and (d) airport wind speeds.

[31] The along-channel density distribution is a key measure of the estuarine dynamics and will be a primary focus of the model-data comparison. Since the density distribution is dominated by salinity in the Chesapeake Bay, we shall employ salinity for comparison. For 1996, we will focus on the April and October measurements because the summer survey was not completed. During the spring months, there was a series of high runoff events so that the April data are representative of the high-runoff period. Runoff was low between June and October, except for a spike in the Potomac River flow in September. Hence the measurements on 1 November are representative of the low-runoff period.

[32] We have run the ROMS model with KPP mixing parameterization using two wind stress fields. One was interpolated directly from the land-based wind measurements obtained at the three airports surrounding the Chesapeake Bay. The other was obtained using the ampli-

fication factors adopted by the Chesapeake Bay Program [c.f. *Xu et al.*, 2002]. The empirical amplification factors were used to represent possible land-sea differences in the wind speed. Figure 14 shows a comparison of along-channel salinity distributions on 1 November 1996, representative of the low-runoff period. Without using the amplification factors, the model produces a stratified surface layer down to 5 m depth (see Figure 14b). Using the amplification factors, the model produces a well-mixed surface layer in better agreement with the observations (compare Figures 14a and 14c). In Figure 21a in section 6, we compared PRNS airport-recorded (near midbay) wind and amplified wind with that observed at the CBOS midbay buoy. It appears that the amplified wind is closer to the buoy wind than the airport wind during this period. The salinity distribution beneath the surface layer shows a general consistency between the model and hydrographic data. The 13 isohaline intercepts the bottom boundary at about 38.8 latitude; the 15 isohaline reaches a location near 38 latitude. However, the model produces weaker stratification in the southernmost portion of the bay (south of 37.2 latitude), although at other times the stratification in the lower bay was reproduced reasonably well (see Figure 16).

[33] While the along-channel salinity distribution is a key metric of estuarine dynamics, salinity distributions in cross-channel sections provide additional views of the three-dimensional field in the Chesapeake Bay estuary. As shown in Figure 8, the monthly-averaged cross-channel salinity distributions show an east-west asymmetry due to the effects of Coriolis force. However, episodic southerly (or northerly) wind events can drive upwelling (or downwelling) flows on the Western Shore and cause isopycnals (isohalines) to make large lateral excursions. Thus the cross-channel salinity distribution is more variable and harder to predict than the along-channel salinity distribution. Figure 15a shows the salinity distribution obtained during a low-bay transect on 13 November 1996. Because the Scansfish was limited to water depths greater than 5 m, the nearshore shoal regions were not sampled. Figure 15a clearly shows the east-west tilt of the isopycnals. In Figure 15b, we plot the modeled salinity distribution at the same location and time. There appears to be a broad consistency between the modeled and observed salinity distributions in this low-bay cross section. Both show the east-west tilt of the isohalines: the brackish 15-salinity water hugs the Western Shore whereas the saline water with salinity at 20 or 21 enters through the deep channel. However, some detailed observed features were not reproduced in the model. Since episodic wind events can easily distort the salinity distribution in cross-channel sections, we need accurate wind forcing in order to obtain reliable predictions for the cross-channel salinity distributions.

[34] Under low-to-medium river discharge conditions discussed above, the model appears to be doing a reasonable job in reproducing the large-scale density structures shown in the observations. How does the model perform under high runoff conditions? Figure 16 shows a comparison of the along-channel salinity distribution on 23 April 1996, representative of the high runoff period. We compared wind speed data between PRNS airport and the midbay CBOS buoy, and found that wind speeds recorded at the CBOS buoy are closer to the original PRNS airport winds than the

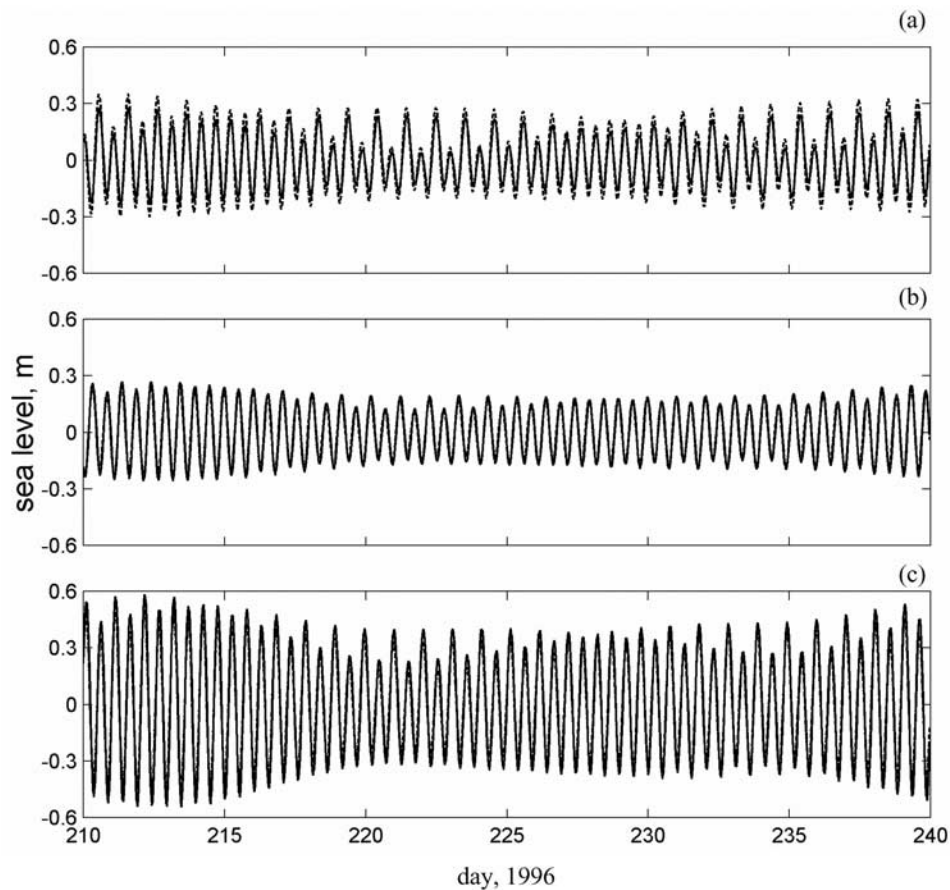


Figure 18. A comparison of predicted (solid line) and observed (dashed line) tidal elevation at three tidal stations: (a) Baltimore, (b) Lewisetta, and (c) CBBT.

amplified values during April 1996 which experienced high winds (see Figure 16a). Hence we shall analyse the results from model runs forced by the original airport winds. We have selected KPP scheme and k-kl scheme with the background diffusivity at $K_{HB} = 10^{-5}$ and $10^{-6} \text{ m}^2 \text{ s}^{-1}$. There appears to be a reasonable agreement on the salinity distribution in the surface layer, down to 10 m depth. Because of the high river flows in April, low-salinity water propagates as a series of bore-like pulses, shown as nearly-vertical isohalines in the surface layer. The salinity increment in the longitudinal direction is quite similar between the model and observations. The agreement of the salinity distribution in the bottom layer (deeper than 10 m depth) is not as good, however. Most noticeably, the halocline situated between 10 and 15 m appears to be much sharper in the observations than in the model. Moreover, the deep high-salinity water in the model does not penetrate as far landward as that shown in the observations.

[35] Even if the background diffusivity is turned down to a low value of $10^{-6} \text{ m}^2 \text{ s}^{-1}$, the model still predicts a more diffuse halocline and weaker stratification than are observed in the estuary. Such discrepancy is probably related to the deficiency of turbulence mixing parameterization schemes in stratified water. As shown in the previous section, all three turbulence closure schemes failed in the stratified interior region and relied on the background diffusivity to generate mixing there. During high runoff periods, turbulent

mixing might be suppressed by fresh water capping saline water. Weaker mixing would have allowed the establishment of stronger stratification in the halocline and further landward penetration of the deep saline water. A time-independent background diffusivity cannot capture intermittent turbulent mixing processes that are established during high runoff periods. Using a background diffusivity that decreases with increasing stratification may improve model prediction. Although the KPP model incorporates a more sophisticated turbulence mixing scheme for breaking internal waves, it did not improve the salinity prediction at lower depths, as shown in Figure 16.

[36] We conducted a similar comparison of the along-channel salinity distribution on 25 April 1997 (see Figure 17). Since the spring runoff is low, vertical stratification is weaker than that in 1996. Nor was a sharp halocline observed. We have compared the observed salinity distribution with two model runs: one forced with the airport winds and the other with the amplified winds. The k-kl turbulence closure scheme was used in these simulations. In Figure 17a we compared wind speeds measured at PRNS airport and at CBOS midbay buoy with the empirically amplified wind speed. Although the buoy wind is in general closer to the airport wind, there are times when the buoy wind lies between the airport and amplified winds, such as on days 117 and 118. The model run forced with the amplified wind generated too much mixing, resulting in a

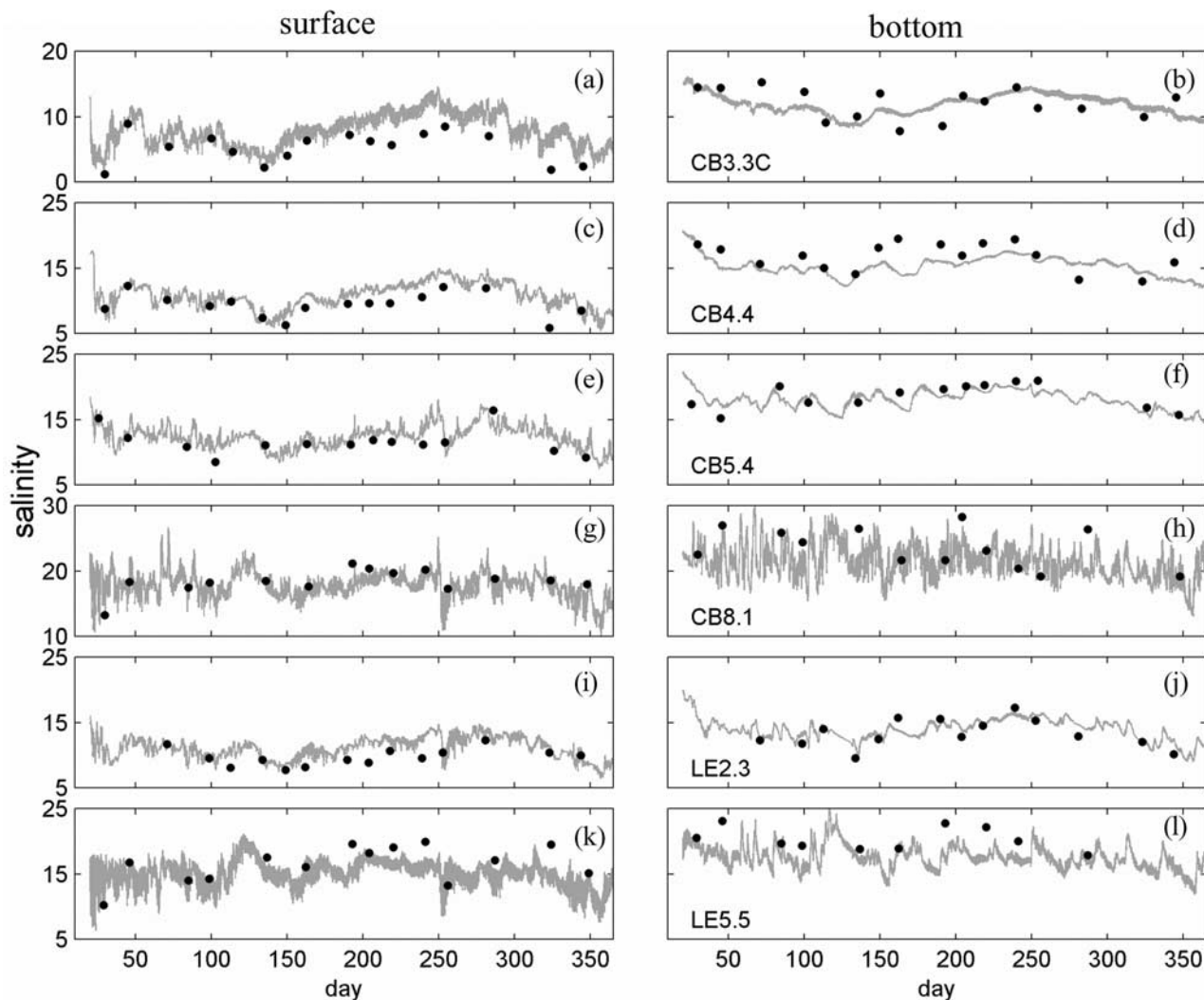


Figure 19. A comparison of modeled (solid lines) and observed (dots) surface/bottom salinity at CBP monitoring stations for the high runoff year of 1996: (a, b) CB3.3, (c, d) CB4.4, (e, f) CB5.4, (g, h) CB8.1, (i, j) LE2.3, and (k, l) LE5.5. Surface salinity is in the left column, and bottom salinity is in the right column.

thick surface mixed layer (see Figure 17c). On the other hand, the model run forced with the airport wind did not generate adequate mixing so that the surface layer remains stratified (see Figure 17c). This model/data comparison underlines another challenge facing numerical modeling of the Chesapeake Bay: the lack of reliable wind-forcing field. Although there are clear land-sea differences in wind speeds, the empirical amplification factors adopted in the CH3D model may not work at all times and should be used with caution. Our comparison between PRNS airport and CBOS midbay buoy winds suggests that the amplification factors are excessive during high wind events. We think that model predictions will be improved if accurate wind data are available to drive the hydrodynamic model.

6. Time Series Comparisons

[37] In the last section we examined snapshots of spatial salinity distributions. To find out how the model captures the temporal variability, we now compare the model results

with observed time series of tidal elevation, salinity and subtidal current speeds at various monitoring stations in the Chesapeake Bay.

[38] To assess the predictive skill of the model, we need a quantitative comparison between the model results and observations. Using the statistical method developed by *Wilmott* [1981], *Warner et al.* [2005b] investigated a measure of the model skill in their simulations of the Hudson River estuary,

$$Skill = 1 - \frac{\sum_{i=1}^N |X_{mod} - X_{obs}|^2}{\sum_{i=1}^N (|X_{mod} - \bar{X}_{obs}| + |X_{obs} - \bar{X}_{obs}|)^2} \quad (5)$$

where X is the variable being compared, \bar{X} its time mean, and the subscripts *mod* and *obs* stand for model results and observations, respectively. This parameter describes the degree to which the observed deviations about the observed

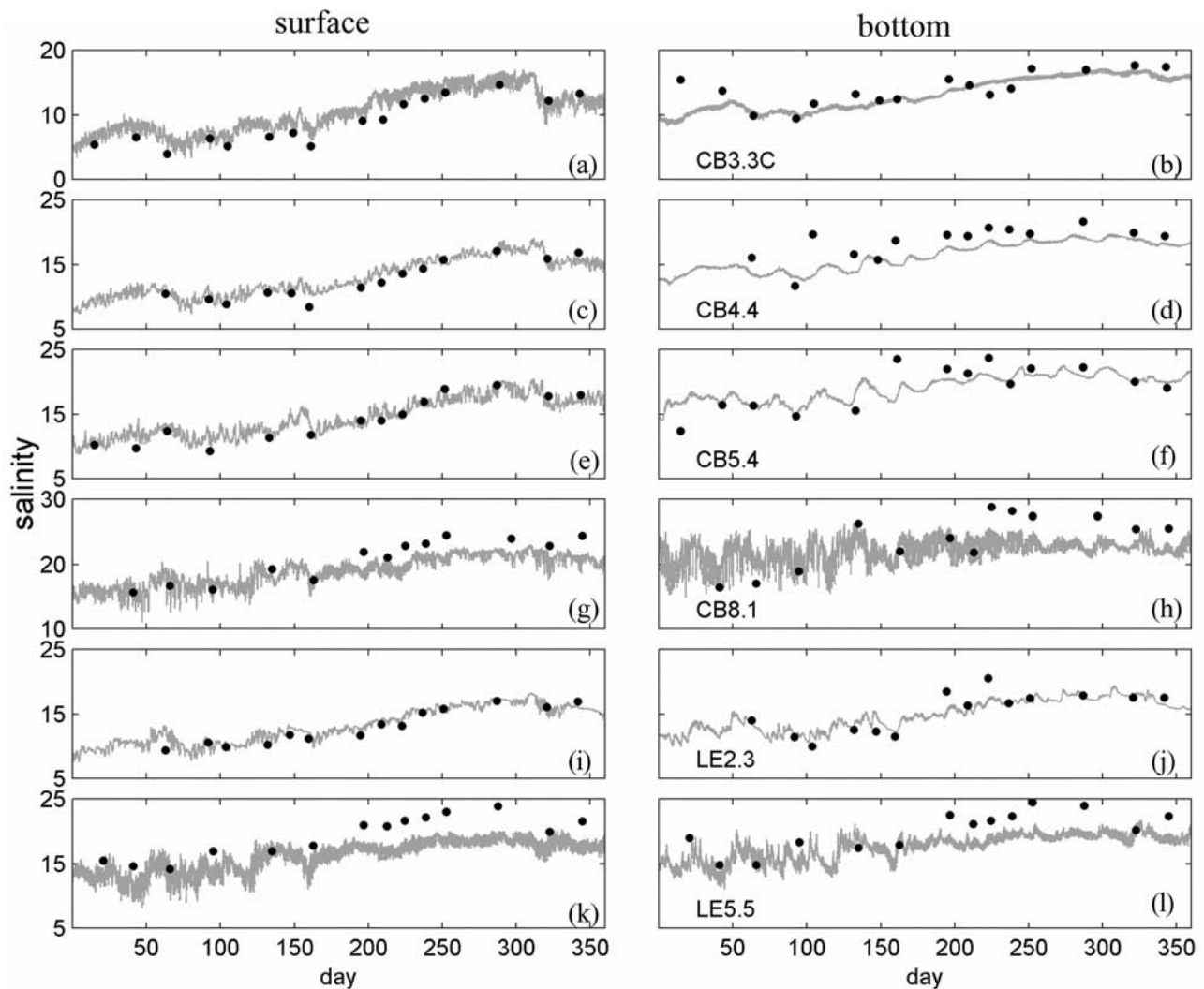


Figure 20. A comparison of modeled (solid lines) and observed (dots) surface/bottom salinity at CBP monitoring stations for the normal runoff year of 1997: (a, b) CB3.3, (c, d) CB4.4, (e, f) CB5.4, (g, h) CB8.1, (i, j) LE2.3, and (k, l) LE5.5. Surface salinity is in the left column, and bottom salinity is in the right column.

mean correspond to the predicted derivations about the observed mean. Perfect agreement between the model results and observations yields a skill of 1.0 whereas complete disagreement yields a skill of 0. We shall use this skill to evaluate prognostics quantities, in addition to examining other statistical measures such as the root-mean square error

$$rms = \left\{ \frac{1}{N} \sum_{i=1}^N (X_{mod} - X_{obs})^2 \right\}^{1/2}. \quad (6)$$

National Ocean Survey (NOS) maintains water-level gauges in the Chesapeake Bay. In Figure 18 we show a comparison of the modeled and observed tidal elevations at three representative stations in the bay. The Baltimore station is located in the upper bay, the Lewisetta station in the mid bay and the CBBT (Chesapeake Bay Tunnel Bridge) station is located near the mouth of the bay (see Figure 1c for their

locations). We conducted a harmonic analysis of water-level records and constructed a time series using the harmonic constants of the five major tidal constituents M_2 , S_2 , N_2 , K_1 and O_1 . As shown in Figure 18, the modeled tidal elevations follow closely the observed records at the lower and middle bay stations, but the model overpredicted tidal amplitude at the Baltimore station in the upper bay. We calculated the skill parameter and found that it is 0.98, 0.99 and 0.99 at the Baltimore, Lewisetta and CBBT stations, respectively. Following *Spitz and Klinck* [1998], we also examined the following error statistics on the tidal prediction: root-mean square (rms) error, relative average error and the correlation coefficient. The RMS error is 4.5 cm, 2.1 cm and 5.4 cm, and the relative average error is 4.5%, 1.2% and 2.0% at the three stations. The correlation coefficient was found to be 0.98, 0.99 and 0.99, respectively, suggesting that the tidal phase is also simulated correctly.

[39] To evaluate how the model captures the temporal variability in salinity, we located four stations in the main

Table 1. Statistics of the Model/Data Comparison for Years 1996 and 1997

		Mean _{obs}	Mean _{mod}	RMS	Skill
<i>Salinity in 1996</i>					
CB3.3C	surface	5.4	8.0	3.0	0.72
	bottom	12.1	11.9	2.1	0.67
CB4.4	surface	9.4	10.6	1.6	0.83
	bottom	16.8	15.4	2.2	0.63
CB5.4	surface	11.6	12.2	1.5	0.78
	bottom	18.6	18.2	1.6	0.75
CB8.1	surface	18.4	17.3	2.6	0.46
	bottom	24.1	22.1	4.1	0.57
LE2.3	surface	9.7	11.1	1.7	0.67
	bottom	13.3	13.9	1.2	0.87
LE5.5	surface	16.5	14.6	2.8	0.70
	bottom	20.8	17.6	4.0	0.46
<i>Salinity in 1997</i>					
CB3.3C	surface	8.9	10.4	2.0	0.92
	bottom	14.0	13.2	2.0	0.82
CB4.4	surface	12.6	13.1	1.0	0.96
	bottom	18.5	16.5	2.7	0.73
CB5.4	surface	14.2	14.6	1.2	0.96
	bottom	19.2	18.8	2.4	0.80
CB8.1	surface	20.8	19.0	2.4	0.84
	bottom	23.8	22.8	2.8	0.77
LE2.3	surface	13.0	13.6	1.1	0.95
	bottom	15.3	15.1	1.7	0.90
LE5.5	surface	19.3	16.2	3.5	0.73
	bottom	20.1	18.0	3.1	0.68
<i>Subtidal Current in 1996</i>					
CBOS	surface	0.07	0.06	0.09	0.78
	bottom	-0.06	-0.05	0.07	0.75
<i>Subtidal Current in 1997</i>					
CBOS	surface	0.08	0.06	0.10	0.82
	bottom	-0.02	-0.07	0.08	0.84

stem: Station CB3.3C, CB4.4, CB5.4 and CB8.1 (see Figure 1c for their locations). They occupy different salinity regimes along the main axis of the bay, ranging from nearly-fresh water in the upper bay to shelf salinity at the bay mouth. In addition, we located one station in each of the two large tributaries: LE2.3 in the Potomac River and LE5.5 in the James River. ROMS uses an orthogonal curvilinear coordinate system. Such a structured grid system does not provide flexibility to place finer resolution in smaller tributaries. By including stations LE2.3 and LE5.5, we can assess model's performance in the tributaries. At each monitoring station, we obtained time series of the surface (about 1 m depth) and bottom (1 to 2 m above the bottom boundary) salinity from the CBP database. To extract the salinity time series from the ROMS model, we located the model grid point closest to a measurement point and interpolated the modeled salinity to the measurement depths. Results presented in Figures 19 and 20 are obtained from the model run forced with the airport winds.

[40] We compare the salinity time series for the high runoff year of 1996 in Figure 19. As expected, seasonal salinity variations are larger at the upper bay stations than at the lower bay stations. At station CB8.1 near the bay mouth, salinity exhibits little seasonal variability but contains large fluctuations at short timescales. These high-frequency fluctuations are possibly due to salinity advection by tidal currents and wind-driven currents [e.g., Valle-Levinson

and Lwiza, 1997]. As shown in Figure 6, steep salinity gradients or density fronts appear near the mouth of bay. Horizontal movements of these fronts can result in large salinity fluctuations at a fixed location. In Table 1 we summarize the statistics of the model/data comparison at the six stations. The model shows reasonable skill scores at stations CB3.3C, CB4.4 and CB5.4. However, the skill score is low at the lower bay station CB8.1, although the RMS errors are about 20% of the mean values. The model does appear to capture the high-frequency variability typical of this high-gradient region in the mouth of the bay, but the biweekly salinity data alias these fluctuations. With a finite grid size, the model would not be expected to produce detailed matching in regions of such strong density gradients. The low skill scores at Station LE5.5 may be due to similar reasons, since Valle-Levinson *et al.* [2000] observed density fronts and lateral flows in the James River. However, the predictive skill at Station LE2.3 in the Potomac River is as good as those in the three main stem stations (CB3.3C, CB4.4 and CB5.4). In addition to the model skill parameter, we calculated statistical quantities such as the mean values and root-mean square (rms) errors. As shown in Table 1, the observed and modeled mean salinity values generally agree within 2 salinity units. However, there are a couple of exceptions. The model overpredicted the mean salinity by 2.6 at Station CB3.3C which is located near the salt wedge in the upper bay. As shown in Figure 5a, there are large horizontal salinity gradients in this region so that a small error in modeling advection could lead to large mismatches in salinity there.

[41] For the more typical runoff year of 1997, the model appears to have captured the seasonal salinity variations well (Figure 20). Most of the skill scores exceed 0.8 and five salinity predictions produce scores above 0.9. Only one score falls below 0.7. These skill scores represent a significant improvement over those in 1996 and suggest that the model did a better job in hindcasting the normal runoff year of 1997 than the high runoff year of 1996. This improvement in model's predictive skill is not unexpected. If we compare the surface-bottom salinity differences using the annual mean values listed in Table 1, we find that the vertical stratification (or top-bottom salinity differences) is significantly weaker in 1997 than in 1996. Therefore a better predictive skill for 1997 is consistent with the result that turbulence mixing parameterization schemes perform better under lower runoff and weaker stratification conditions.

[42] Another important metric for evaluating model results is the subtidal residual velocity. Time series current observations were made at the Chesapeake Bay Observing System (CBOS) midbay station located in the deep channel of the bay, approximately 100 km seaward of the Susquehanna River mouth (see Figure 1c for its location). This position has been found to be representative of the longitudinal flow in the Deep Trough of the bay, which extends from 60 km to 210 km seaward of the River mouth. Typically, two fixed depth conventional current meters were employed to obtain flow measurements at 2.4 and 19 m depths. To understand the subtidal variability of both observations and model, we produce a stack plot of axial velocity and winds for the month of October in the high runoff year of 1996 (Figure 21). Both observations and

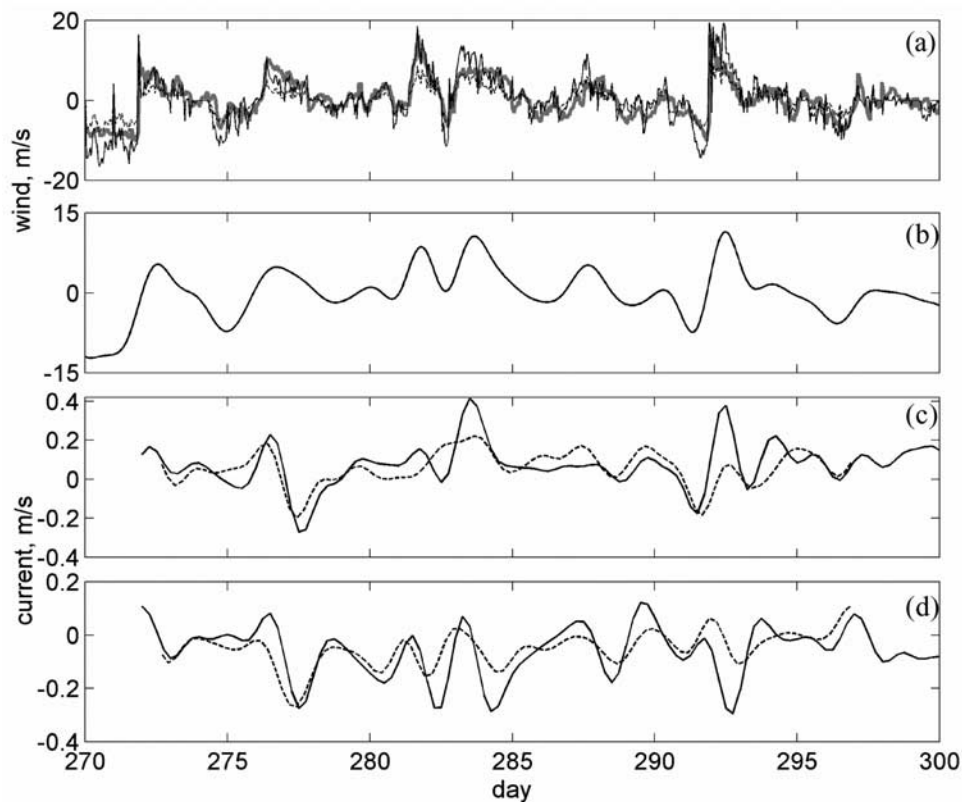


Figure 21. Comparison of the subtidal velocity between the ROMS model and CBOS observations at the midbay station during the fall of 1996. (a) Time series of the empirically adjusted wind speed used to drive the ROMS model (solid line) and its comparison with the along-channel wind speed measured at PRNS airport (dashed line) and CBOS buoy (thick shaded line). Positive values correspond to northerly winds. (b) Low-pass filtered wind speed. Low-pass filtered along-channel current speed (positive for the seaward direction) at (c) 2.4 and (d) 19 m depth. The solid line represents CBOS observations, and the dashed line represents the ROMS predictions.

model records were passed through a 34-hour Lanczos filter to remove tidal fluctuations. Positive values correspond to northerly winds. We have run the model using both the original airport winds and the empirically amplified winds. Currents predicted in the model are sensitive to the specification of wind forcing. The model run forced with the original airport winds produces current speeds significantly weaker than the observed values. In Figure 21a, we compare the airport-recorded and the amplified wind speeds with that observed at the CBOS midbay buoy. The amplified wind appears to be closer to the buoy wind. Figures 21c and 21d show considerable variability in subtidal velocity in the Chesapeake Bay. When averaged over the monthly record shown in Figure 21, the observed current shows a net seaward flow of 0.07 m s^{-1} at 2 m depth and a net landward flow of 0.06 m s^{-1} at 19 m depth, consistent with the two-layer gravitational circulation. However, short-term wind events drove currents which had a magnitude of up to 0.4 m s^{-1} and sometimes moved in a direction opposite to the gravitational circulation. Since the model smooths out topographic features smaller than its grid size, it will generate Eulerian flows which will differ from the observed currents, which respond to small local topographic influences, especially in the lower layer. Nevertheless, the model appears to track the phase of velocity fluctuations reason-

ably well. Phase discrepancies do not appear to be consistently biased toward either lead or lag. The model also appears to reproduce the velocity magnitude during low-to-moderate wind events. However, the model underpredicted the current speed during the strong northerly wind events on day 283 and 293. Northerly winds drive fresh water seawards, resulting in stronger stratification in the water column and weaker turbulent momentum exchange between the surface and bottom layers. Wind-driven currents will be stronger in an uncoupled two-layer system. It appears that the turbulence mixing schemes used in ROMS produces too much mixing and turbulent momentum flux in the vertical direction, leading to weaker current response to the wind-forcing. In Table 1, we list the statistics for the subtidal velocities. The model predictive skill is 0.78 and 0.75 for the surface and bottom subtidal velocities, respectively.

[43] We carried out the same comparison of the subtidal velocity over a 40-day period during the normal runoff year of 1997 (Figure 22). There were a series of strong wind events, each lasting for 2 to 5 days, as shown in both the original and filtered winds. The Chesapeake Bay responded to this local longitudinal wind-forcing [Wang, 1979a], with amplitude and duration of currents matching those in the wind record reasonably well. Figure 22 suggests that the modeled currents track the observed current, but there were

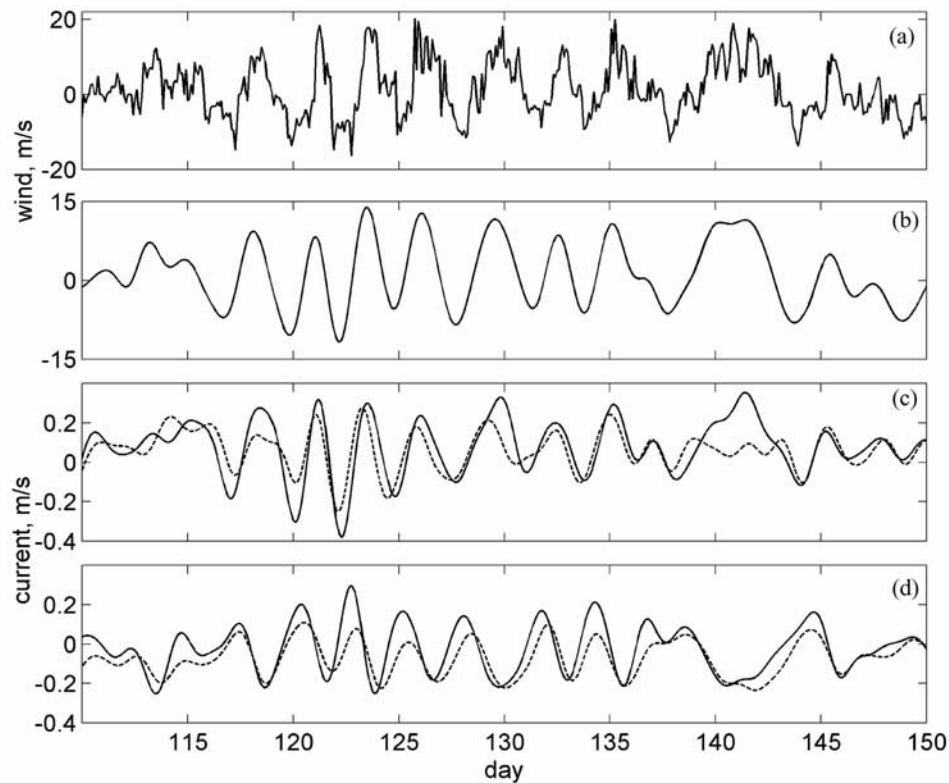


Figure 22. Comparison of the subtidal velocity between the ROMS model and CBOS observations at the midbay station during the spring of 1997. (a) Time series of the empirically adjusted wind speed used to drive the ROMS model. (b) Low-pass filtered wind speed. Low-pass filtered along-channel current speed (positive for the seaward direction) at (c) 2.4 and (d) 19 m depth. The solid line represents CBOS observations and the dashed line represents the ROMS predictions.

small but visible phase differences. The model skill is 0.82 and 0.84 for the surface and bottom subtidal velocities, respectively. The scores would have been higher if the phases were matched better.

7. Conclusions

[44] We used ROMS to make hindcast simulations of the Chesapeake Bay estuary over a 2-year period covering both an unusually wet year and a more typical runoff year. Model results were compared with time series measurements and high-resolution salinity distributions from towed undulating vehicles. The model shows skill in reproducing observed temporal variability in sea level height, salinity and subtidal current. Predictive skill is appreciably better for the normal runoff year of 1997 than for the high runoff year of 1996. The model qualitatively reproduces the axial and lateral salinity distributions during low to medium runoff periods, but produces weaker stratification and a more diffuse halocline than the observations during high runoff periods. Model/data comparisons show that the model simulations are less accurate under strong stratification conditions. This degradation in the model's predictive skill is likely related to the deficiency of turbulence parameterization schemes in handling strong stratification.

[45] We have also examined the sensitivity of model results to turbulence mixing parameterization and experi-

mented with four turbulence closure schemes (Mellor-Yamada, $k-\epsilon$, $k-\omega$ and KPP models). Little difference was found in the model results between the different schemes. However, vertical stratification shows a strong sensitivity to the background diffusivity, because the vertical diffusivity inferred from the model is found to be set by the background diffusivity except in the surface and bottom boundary layers. The model sensitivity studies have shown that these turbulence parameterization schemes are doing a reasonable job of simulating turbulent mixing in the bottom and surface boundary layers but all appear to have failed to produce an eddy diffusivity above the background level in the interior of water column. In ROMS and other coastal ocean models, the constant background diffusivity is often used to parameterize unresolved mixing processes such as breaking internal waves. Although the background diffusivity can be adjusted to match the modelled and observed stratification under certain circumstances, it did not work during the high-runoff period in our model simulations. The background diffusivity may need to be turned down at times when the strong stratification is established to suppress vertical mixing.

[46] Both the model sensitivity study and model/data comparison have demonstrated the importance of obtaining a more realistic parameterization for turbulence mixing under strong stratification conditions. Many previous investigations have focused on turbulent mixing in tidal bound-

ary layers so that the turbulence models can now simulate it reasonably well. As Geyer and Smith [1987] demonstrated, however, intermittent mixing in the pycnocline is a principal mechanism for transporting salt and other materials vertically in estuaries. Our paper reinforces their point and calls for more investigation into turbulent mixing in the stratified pycnocline. Although the interior mixing may be related to the entrainment of the boundary layers into the pycnocline region, the processes responsible for propagation of energy into the interior are not represented in the turbulent closure models. In particular, the closure models do not explicitly account for the vertical transport of second-order turbulent quantities in the transition zone between the boundary layer and pycnocline. Our model results are consistent with other recent modeling studies. For example, Warner *et al.* [2005b] noted that the stratification in their model tends to extend all the way to the water surface whereas the observations indicate a distinct pycnocline and a surface mixed layer.

[47] Better wind-forcing data are needed to improve the predictive capability of the hydrodynamic model for the Chesapeake Bay. Our numerical experiments have shown that the near-surface stratification and subtidal current are sensitive to wind-forcing. Wind speeds recorded at the land-based airports generally underpredict those over the bay's surface, but the empirical amplification factors appear to be excessive during high wind periods, leading to too much mixing in the water column. NOAA is working with the academic community in the Chesapeake Bay region to make comprehensive wind measurements over the bay surface. These new measurements will help develop more accurate wind-forcing field for the hydrodynamic model. Alternatively, we could consider using wind products from regional weather forecasting models. Once validated against sea-based measurements, these wind data would provide a wind field with high temporal and spatial resolutions over the Chesapeake Bay.

[48] **Acknowledgments.** We thank three anonymous referees for their helpful comments and Carole Derry for her help in processing CBOS data. We also thank Dale Haidvogel and Hernan Arango for helpful discussions on the ROMS model. We thank the Chesapeake Bay Program for providing salinity data at its monitoring stations and NOAA for providing sea level data at the tidal gauges. This work is supported by a grant from NOAA/CICEET. The TIES project was supported by NSF. In addition, NSF contributed to CBOS. This is UMCES contribution 3892.

References

- Blumberg, A. F., and D. M. Goodrich (1990), Modeling of wind-induced destratification in Chesapeake Bay, *Estuaries*, *13*, 236–249.
- Boicourt, W. C. (1992), The influences of circulation processes on dissolved oxygen in Chesapeake Bay, in *Dissolved Oxygen in Chesapeake Bay*, edited by D. Smith, M. Leffler, and G. Mackiernan, pp. 7–59, Md. Sea Grant, College Park, MD.
- Browne, D. R., and C. W. Fisher (1988), Tide and tidal currents in the Chesapeake Bay, *NOAA Tech. Rep. NOS OMA 3*, 84 pp., Natl. Oceanic and Atmos. Admin., Silver Spring, Md.
- Burchard, H., O. Petersen, and T. Rippeth (1998), Comparing the performance of the Mellor-Yamada and the $k-\epsilon$ two equation turbulence models, *J. Geophys. Res.*, *103*, 10,543–10,554.
- Carter, H. H., and D. W. Pritchard (1988), Oceanography of Chesapeake Bay, in *Hydrodynamics of Estuaries: Dynamics of Partially-Mixed Estuaries*, vol. 1, edited by B. Kjerfve, pp. 1–16, CRC Press, Boca Raton, Fla.
- Chao, S.-Y., and W. C. Boicourt (1986), Onset of estuarine plumes, *J. Phys. Oceanogr.*, *16*, 2137–2149.
- Deardorff, J. W. (1972), Theoretical expression for the counter-gradient vertical heat flux, *J. Geophys. Res.*, *77*, 5900–5904.
- Durski, S. M., S. M. Glenn, and D. B. Haidvogel (2004), Vertical mixing schemes in the coastal ocean: Comparison of the level 2.5 Mellor-Yamada scheme with an enhanced version of the K profile parameterization, *J. Geophys. Res.*, *109*, C01015, doi:10.1029/2002JC001702.
- Gargett, A. E., and G. Holloway (1984), Dissipation and diffusion by internal wave breaking, *J. Mar. Res.*, *42*, 15–27.
- Geyer, W. R., and J. D. Smith (1987), Shear instability in a highly stratified estuary, *J. Phys. Oceanogr.*, *17*, 1668–1679.
- Goodrich, D. M. (1985), On stratification and wind-induced mixing in the Chesapeake Bay, Ph.D. thesis, 134 pp., State Univ. of New York at Stony Brook, Stony Brook, N. Y.
- Goodrich, D. M. (1988), On meteorologically induced flushing in three U.S. East Coast estuaries, *Estuarine Coastal Shelf Sci.*, *26*, 111–121.
- Goodrich, D. M., and A. F. Blumberg (1991), The fortnightly mean circulation of Chesapeake Bay, *Estuarine Coastal Shelf Sci.*, *32*, 451–462.
- Goodrich, D. M., W. C. Boicourt, P. Hamilton, and D. W. Pritchard (1987), Wind-induced destratification in Chesapeake Bay, *J. Phys. Oceanogr.*, *17*, 2232–2240.
- Gregg, M. C. (1987), Diapycnal mixing in the thermocline: A review, *J. Geophys. Res.*, *92*, 5249–5286.
- Haidvogel, D. B., H. G. Arango, K. Hedstrom, A. Beckmann, P. Malanotte-Rizzoli, and A. F. Shchepetkin (2000), Model evaluation experiments in the North Atlantic Basin: Simulations in nonlinear terrain-following coordinates, *Dyn. Atmos. Oceans*, *32*, 239–281.
- Harding, L. W., Jr., M. E. Mallonee, and E. S. Perry (2002), Toward a predictive understanding of primary productivity in a temperate, partially stratified estuary, *Estuarine Coastal Shelf Sci.*, *55*, 437–463.
- Ippen, A. T. (1966), Tidal dynamics in estuaries: Part I. Estuaries of rectangular section, in *Estuary and Coastline Hydrodynamics*, edited by A. T. Ippen, pp. 493–522, McGraw-Hill, New York.
- Johnson, B. H., K. W. Kim, R. E. Heath, N. N. Hseish, and H. L. Butler (1993), Verification of a three-dimensional hydrodynamic model of Chesapeake Bay, *J. Hydraul. Eng.*, *119*, 2–20.
- Kantha, L. H., and C. A. Clayson (1994), An improved mixed layer model for geophysical applications, *J. Geophys. Res.*, *99*, 25,235–25,266.
- Kato, H., and O. M. Phillips (1969), On the penetration of a turbulent layer into stratified fluid, *J. Fluid Mech.*, *37*(4), 643–655.
- Large, W. G., J. C. Williams, and S. C. Doney (1994), Oceanic vertical mixing: A review and a model with a nonlocal boundary layer parameterization, *Rev. Geophys.*, *32*(4), 363–403.
- Ledwell, J. R., A. J. Watson, and C. B. Law (1993), Evidence for slow mixing across the pycnocline from an open-ocean tracer-release experiment, *Nature*, *364*, 701–703.
- Levitus, S. (1982), Climatological atlas of the world ocean, *NOAA Prof. Pap. 13*, 173 pp., Natl. Oceanic and Atmos. Admin., Silver Spring, Md.
- MacCready, P., and W. R. Geyer (2001), Estuarine salt flux through an isohaline surface, *J. Geophys. Res.*, *106*, 11,629–11,637.
- MacCready, P., R. D. Hetland, and W. R. Geyer (2002), Long-term isohaline salt balance in an estuary, *Cont. Shelf Res.*, *22*, 1591–1601.
- Marchesiello, P., J. C. McWilliams, and A. F. Shchepetkin (2001), Open boundary conditions for long-term integration of regional ocean models, *Ocean Modell.*, *3*, 1–20.
- Marchesiello, P., J. C. McWilliams, and A. F. Shchepetkin (2003), Equilibrium structure and dynamics of the California Current System, *J. Phys. Oceanogr.*, *33*, 753–783.
- Mellor, G. L., and T. Yamada (1982), Development of a turbulence closure model for geophysical fluid problems, *Rev. Geophys.*, *20*(4), 851–875.
- Monismith, S. G., J. R. Burau, and M. T. Stacey (1996), Stratification dynamics and gravitational circulation in northern San Francisco Bay, in *San Francisco Bay: The Ecosystem*, edited by T. Hollibaugh, pp. 123–153, Am. Assoc. for the Adv. of Sci., Washington, D. C.
- Munk, W. H. (1966), Abyssal recipes, *Deep Sea Res.*, *13*, 707–730.
- Rodi, W. (1987), Examples of calculation methods for flow and mixing in stratified fluids, *J. Geophys. Res.*, *92*, 5305–5328.
- Simpson, J. H., and J. Sharples (1991), Dynamically-active models in the prediction of estuarine stratification, in *Dynamics and Exchanges in Estuaries and the Coastal Zone*, edited by D. Prandle, pp. 101–113, Springer, New York.
- Song, Y. T., and D. B. Haidvogel (1994), A semi-implicit ocean circulation model using a generalized topography-following coordinate, *J. Comput. Phys.*, *115*, 228–244.
- Spitz, Y. H., and J. M. Klinck (1998), Estimate of bottom and surface stress during a spring-neap tide cycle by dynamic assimilation of tide gauge observations in the Chesapeake Bay, *J. Geophys. Res.*, *103*, 12,761–12,782.
- Umlauf, L., and H. Burchard (2003), A generic length-scale equation for geophysical turbulence models, *J. Mar. Res.*, *61*, 235–265.
- Umlauf, L., H. Burchard, and K. Hutter (2002), Extending the k -model towards oceanic applications, *Ocean Modell.*, *5*, 195–218.

- Valle-Levinson, A., and K. M. M. Lwiza (1995), The effects of channels and shoals on exchange between the Chesapeake Bay and the adjacent ocean, *J. Geophys. Res.*, *100*, 18,551–18,563.
- Valle-Levinson, A., and K. M. M. Lwiza (1997), Bathymetric influences on the lower Chesapeake Bay hydrography, *J. Mar. Syst.*, *12*, 221–236.
- Valle-Levinson, A., C. Li, K. C. Wong, and K. M. M. Lwiza (2000), Convergence of lateral flow along a coastal plain estuary, *J. Geophys. Res.*, *105*, 17,045–17,061.
- Vieira, M. E. C. (1986), The meteorologically driven circulation in mid-Chesapeake Bay, *J. Mar. Res.*, *44*, 473–493.
- Wang, D.-P. (1979a), Subtidal sea level variations in the Chesapeake Bay and relation to atmospheric forcing, *J. Phys. Oceanogr.*, *9*, 413–421.
- Wang, D.-P. (1979b), Wind-driven circulation in the Chesapeake Bay, winter 1975, *J. Phys. Oceanogr.*, *9*, 564–572.
- Wang, H. V., and B. J. Johnson (2000), Validation and application of the second generation three dimensional hydrodynamic model of Chesapeake Bay, *Water Qual. Ecosyst. Model.*, *1*, 51–90.
- Warner, J. C., C. R. Sherwood, H. G. Arango, B. Butman, and R. P. Signell (2005a), Performance of four turbulence closure models implemented using a generic length scale method, *Ocean Modell.*, *8*, 81–113.
- Warner, J. C., W. R. Geyer, and J. A. Lerczak (2005b), Numerical modeling of an estuary: A comprehensive skill assessment, *J. Geophys. Res.*, *110*, C05001, doi:10.1029/2004JC002691.
- Wijesekera, H. W., J. S. Allen, and P. A. Newberger (2003), Modeling study of turbulent mixing over the continental shelf: Comparison of turbulence closure schemes, *J. Geophys. Res.*, *108*(C3), 3103, doi:10.1029/2001JC001234.
- Wilcox, D. C. (1988), Reassessment of the scale-determining equation for advanced turbulence models, *AIAA J.*, *26*(11), 1299–1310.
- Wilmott, C. J. (1981), On the validation of models, *Phys. Geogr.*, *2*, 184–194.
- Xu, J., S.-Y. Chao, R. R. Hood, H. Wang, and W. C. Boicourt (2002), Assimilating high-resolution salinity data into a model of a partially mixed estuary, *J. Geophys. Res.*, *107*(C7), 3074, doi:10.1029/2000JC000626.

W. C. Boicourt, M. Li, and L. Zhong, Horn Point Laboratory, University of Maryland Center for Environmental Science, P.O. Box 775, Cambridge, MD 21613, USA. (mingli@hpl.umces.edu)